# Finding Faults in the Charleston Area, South Carolina: 1. Seismological Data

Inmaculada Durá-Gómez and Pradeep Talwani

**Abstract**
Macroscopic observations following the 1886 Charleston South Carolina earthquake and analyses of instrumentally recorded seismicity between 1974 and 2004 suggest the presence of two or more active faults. In order to more clearly define the active faults and determine their seismotectonic framework, instrumentally located hypocenters were relocated using the double-difference algorithm HypoDD. The revised hypocentral locations were associated with different faults based on the first motions recorded at different locations. The result is a plausible framework which shows several important changes from earlier interpretations. This framework defines a localized stressed volume which consists of ~50 km long ~N30°E striking, NW dipping Woodstock fault associated with oblique right-lateral strike-slip motion with a ~6 km long antidilational left step near Middleton Place. Three ~NW-SE striking, two NE dipping and one SW dipping, reverse faults were recognized within this left step, of which, the NE dipping Sawmill Branch Fault zone lying between Middleton Place and Summerville is the most active. Minor activity was observed on the NE dipping Lincolnville and the SW dipping Charleston faults. The southernmost Sawmill Branch Fault zone also shows evidence of left-lateral strike-slip motion. The ~N55°W trending Ashley River fault lying between Middleton Place and the Magnolia Plantation appears to be currently inactive .

## 1. Introduction

The aim of this and the companion paper is to present a revised, plausible seismogenic framework to explain the 1886 and ongoing seismic activity near Charleston, South Carolina. The exact nature of these faults was largely unknown because the earthquakes occur below subsurface Triassic age basalt flows and the general absence of a surface expression of faults. However, in the past three decades a variety of multidisciplinary data have become available, and have led to an improved understanding of surface and subsurface features that may be related to the seismicity. In this paper we present a plausible seismotectonic framework based on the analysis of seismicity data collected over three decades, complemented and constrained by geological, geophysical, geomorphological and

geodetic data. The details of these complementary data are presented in the companion paper.

The earliest information about the seismic sources in the Charleston seismic zone came from the several descriptions of the macroscopic effects of the 1886 Charleston earthquake. They indicated that the seismicity was associated with multiple sources. These data are described in the next section. The next advance in our understanding occurred in the early 1970s with the deployment of a seismic network in the Charleston region. As the number and accuracy of hypocentral locations improved, so did our ideas of the causative faults. These improvements in the development of a seismogenic framework occurred in parallel with improvements in our understanding of the nature of intraplate earthquakes. These are described in the following sections and are the subject of this paper.

**2. Inferences of multiple sources from the reports of the 1886 Charleston earthquake.**

The idea of the presence of multiple faults in the Summerville area dates back to the studies carried out after the 1886 Charleston earthquake. Clarence E. Dutton, Captain of the U.S. Ordnance Corps in charge of the earthquake investigation for the U.S. Geological Survey, Division of Volcanic Geology, compiled a report that included the first-hand accounts by C. McKinley, G.E. Manigault and F.R. Fisher (Dutton, 1890). Many of these accounts described a SW-NE direction of motion in Charleston while chronicles in the Summerville area described mainly vertical motions. According to McKinley, associate Editor of the *Charleston News and Courier*, on James Island, located a few miles south of Charleston, "the direction of the motion was reported to have been from the southwest, passing off towards the north" (Dutton, 1890, p. 224). Dr. Manigault, curator of the College of Charleston whose residence was located in the southwestern part of Charleston on the bank of the Ashley River, reported that his "impression as to the direction from which the

waves came was that they reached me from a little south of west by the compass, and that they traveled to a little north of east" (Dutton, 1890, p. 240-241). In Summerville, vertical motion was extensively reported. Dr. Manigault wrote that "…these indications of what was coming were more distinct at the village of Summerville, about twenty miles from Charleston, on the line of the railroad to Augusta, Ga., and more distinct still at "Ten Mile Hill", on the same railroad; as both those places, especially the first, were afterwards the scenes of vertical thrusts" (Dutton, 1890, p. 231). Other felt reports from Summerville compiled by Dutton described that "…for the direction of its impulses was nearer the vertical than the horizontal… The injuries to chimneys were also very characteristic. … in many cases, instead of being snapped off clean by a horizontal fracture, were broken along a highly inclined plane, as if sheared, and fell easily to the ground. There was a marked tendency to fall in a northwestern and southeastern direction, but instances could be found of chimneys falling in almost any direction" (Dutton, 1890, p. 274). Among these felt reports, one written by Mr. Thomas Turner, president of the Charleston Gas Light Company, mentions that "…the floor seemed to go down in front of me at an angle of twenty-five to thirty degrees. It was so sudden and unexpected, that I was thrown forward into the hall about 10 feet and as quickly thrown backwards..." (Dutton, 1890, p. 272)

More than one active fault in the area is also suggested by the entries in the diary of Ada Trotter. Ms. Trotter, an Englishwoman familiar with earthquakes from her stay in Italy, and who visited Summerville between March 18, 1887 and May 2, 1888, kept a journal of the still frequent aftershocks (Louderback, 1943). There was continuing, audible seismicity that she associated with two different sources, one near and one distant. She usually described the earthquakes originated in the nearby source as loud explosions under the house. For example, on March 24, 1887, she wrote: "Was sitting in the Piazza when an explosive kind of

rumbling sounded right under me. My chair shook slightly and I saw the Piazza was shaken too. Mr. Boyle came over and said he felt the earth move under his feet and that there was something very unusual in the character of the shake. Seems to me as though there was a dynamite factory in operation immediately under us and occasional explosions" Other entries in the diary relate to earthquakes coming from a more distant source. For example, on March 28, 1887, she wrote: "Near morning I think, but while it was quite dark, I was wakened by a loud rumbling and very slight shake. Scarcely five minutes later came a louder bang and quite a long shake though gentle. My bed shook back and forth, east and west. Things in the room rattled".

Adding to the story of Ada Trotter is the fact that she distinguished two different directions of shaking which could be associated with two separate seismic sources. On April 14, 1887, she wrote: "Last night, (Wed. night) at 2:25 a rumbling and vigorous shake from north to south instead of as usual east to west. Was told this morning that a bomb! went off a little earlier, this is what probably awoke me, for I was awake when the one I record occurred".

First hand accounts also brought up the possibility that the main shock was a "compound" shock. Dr. Manigault expressed to C. E. Dutton (Manigault in Dutton, 1890) that "The impression produced upon many was that it could be subdivided into three distinct movements, while others were of the opinion that it was one continuous movement or succession of waves". Earle Sloan, a mining consultant at the time of the earthquake and named assistant USGS geologist, explained the event as a compound shock with three epicenters, the first near the town of Woodstock, the second near Middleton Place (on the bank of the Ashley River) and the third west of Rantowles (map in McKinley, 1887). Dutton

reinterpreted the data gathered by Earle Sloan and concluded that the seismicity was associated with two seismic sources, located near Woodstock and Rantowles (Figure 1).

**3. Modern Era**

During the twentieth century, various researchers have studied the causes of the 1886 Charleston earthquake. Their studies and conclusions are summarized in this section.

Taber (1914) suggested the August 31, 1886 earthquake was caused by differences in rainfall in the preceding months between Summerville and Charleston. The larger amount of rainfall near Summerville resulted in "readjustments taking place along a plane of faulting located in the crystalline basement underlying the Coastal Plain sediments, not far from Woodstock, and extending in a general northeast-southwest direction" (Figure 1).

Bollinger (1977) reassessed the 1886 earthquake intensity data to obtain two new isoseismals maps (on the Modified Mercalli Intensity scale) emphasizing the broad regional pattern of effects and the more localized variations of intensity, respectively. While previous intensity contours by Sloan as cited in Dutton, had not been labeled, Bollinger assigned intensity values to his contours and estimated that the maximum epicentral intensity was X on the Modified Mercalli Intensity Scale. In addition, he estimated the body-wave magnitude to be 6.8 based on intensity-particle velocity data derived from Central U.S data or 7.1 based on Western U.S. data. Assuming the value of 6.8 for the body-wave magnitude, he estimated the fault length, fault width and average slip to be 25 km, 12 km and 1 m respectively (Bollinger, 1983). Current estimates of the magnitude of the 1886 earthquake, based on isoseismal data, range between $M_W$7.3 and 6.9 (Johnston, 1996; and Bakun and Hoper, 2004 )

The South Carolina Seismic Network (SCSN) was established in 1974. After analyzing the instrumentally recorded seismicity (1973 to 1979) in the South Carolina Coastal Plain, Tarr et al. (1981) defined three clusters of seismicity: Middleton Place-Summerville

Seismic Zone (MPSSZ), (Figure 2) the most active; Bowman Seismic Zone (BSZ); and Adams Run cluster, herein renamed the Adams Run Seismic Zone (ARSZ). Tarr and Rhea (1983) identified the MPSSZ as the source of the 1886 Charleston earthquake. A variety of fault plane solutions available for the area led Talwani (1982) to consider the possibility of more than one active fault. Talwani (1982) revised the velocity model under MPSSZ, relocated the earthquakes occurring between 1974 and 1980, and defined two faults: the NW-SE trending Ashley River fault (ARF) associated with high-angle reverse faulting, and the NNE-SSW trending Woodstock fault (WF, named after Taber's (1914) original suggestion), associated with right-lateral strike-slip movement. He extended the WF southwest to the ARSZ based on the 1967 M3.4 earthquake (Dewey, 1983) located between MPSSZ and ARSZ (Figure 2). He inferred a N60ºE direction of maximum horizontal compression from the composite fault plane solutions obtained for these earthquakes, later confirmed by Zoback (1983) from studies of well breakout data at the Clubhouse Crossroads deep borehole.

Representative fault plane solutions for two well-located earthquakes, with an epicentral separation of less than 5 km and hypocentral difference of less than 1 km, show remarkably different styles of faulting. The M 4.1 event on August 21, 1992 (32.984ºN, 80.168ºW, 8.0 km) was associated with reverse faulting on a N22ºW striking plane, whereas the M 2.3 event on July 22, 2001 (32.9587ºN, 80.1747ºW, 7.0 km) was associated with primarily right-lateral strike-slip on a N17ºE striking fault plane (Figure 2). The inferred direction of the P-axes for the two fault plane solutions are oriented N70ºE and N60ºE respectively.

After the identification of two possible faults based on their focal mechanisms and hypocentral distribution (Talwani, 1982), subsequent studies further strengthened the

observation that there may be multiple faults associated with the seismicity in MPSSZ. Shedlock (1987, 1988) revised the earthquake locations from 1974 to 1986 by using a three dimensional velocity structure. She found hypocenters located as deep as 10 to 12 km in the MPSSZ, with the deeper events located on the west side of the zone and the shallower along the east side of the zone. The fault plane solutions indicated thrust, strike-slip and normal faulting. She found that the maximum horizontal compressive stress SHmax was oriented NE-SW for events shallower than 9 km and E-W for events from 9 to 12 km deep.

Madabhushi and Talwani (1993) evaluated the instrumental seismicity data from 1980 to 1991. They identified three main groups of earthquakes: the first was associated with the Ashley River fault (ARF) zone (reverse faulting on NW-SE striking, SW dipping fault planes); the second, associated with the Woodstock fault (WF) zone (right-lateral strike-slip motion on NNE-SSW striking vertical faults); and the third, associated with both the ARF and WF zones, suggesting an intersection of these two fault zones.

Garner (1998) re-evaluated the seismicity data from 1974 to 1996 by improving the hypocentral locations and segregating the data into two main groups based on their focal mechanisms and depth distribution. He defined two fault planes: the first, a N10ºE striking Woodstock fault, discontinuous, with a left step, offset south of Summerville, along the second fault, ~NW striking Ashley River fault plane with a ~65º SW dip.

Durá-Gómez (2004) reviewed the seismotectonic framework of the MPSSZ. She improved the hypocentral locations from 1974 to 2003 and compared them with the results of various geological and geophysical investigations. Her results indicated that the seismogenic structures are located between 3 km and 12 km in depth and most of the seismicity is located to the northwest of Middleton Place (Figure 2). She divided the originally defined Ashley River fault, extending from the Magnolia Plantation to

Summerville, into two parts: a seismically active ~N30ºW oriented Sawmill Branch fault (SBF) with a strong reverse component and a dip of about 70º to the southwest, and the ~N50º-60ºW, essentially aseismic fault along the Ashley River between Middleton Place and the Magnolia Plantation, for which the name Ashley River fault was retained (Figure 2). Her analysis supported the presence of an offset in the Woodstock fault, with the southern arm, oriented ~N30ºE and roughly parallel to the northern arm. The strike of the southern arm of WF was based on the seismicity near the Adams Run Seismic Zone, on the epicenter of the October 23, 1967 M 3.4 earthquake obtained by Dewey (1983) and on the focal mechanism of a cluster of events obtained by Talwani (1982). Based on the seismicity, seismic reflection and geomorphic data the strike of the Woodstock fault varied from about N30ºE to N20ºE (Figure 2).

The above observations, different focal mechanisms and sounds emanating from the epicentral area suggest the presence of multiple faults. Further, most of the nodal planes obtained from the fault plane solutions are not very well constrained (strike uncertainty > 15°) and because of the fact that the faults in this area do not have a surface expression, discerning the seismotectonic framework relies on indirect evidence. Both the epicentral (Figure 2) and the hypocentral distributions (Durá-Gómez, 2004) do not lend themselves to any obvious division of hypocenters into distinct fault planes. So it was considered necessary to try and further improve the relative locations of the hypocenters using HypoDD (Waldhauser and Ellsworth, 2000) before trying to delineate multiple fault planes.

**4. Relocation of earthquakes using HypoDD**

Seismicity in the MPSSZ is mainly concentrated in a ~30x20 $km^2$ area between Summerville and Middleton Place (Figure 2). Seismic stations of the South Carolina Seismic Network (SCSN) (Figure 3) are concentrated around this pocket of seismicity, providing

very good azimuthal coverage except for earthquakes located to the north of Summerville (Figure 3). For the period 1974-2004, 294 earthquakes with M≥0.4 were located using HYPOELLIPSE (Lahr, 1996). These earthquakes were located by using a modification of the 1-D velocity model, originally developed by Talwani (1982) (Table 1). In this model, the depth of the sedimentary section, its P-wave velocity and its Vp/Vs ratio (2.93) were obtained from sonic logs in a borehole in the epicentral area. Shallow refraction data (down to 3-4 km) from three reversed profiles were combined with P-wave phases for 21 well located earthquakes and inverted using the program VELEST (Ellsworth, 1977) to obtain the velocity model. Please see Talwani (1982) for details. Station corrections were estimated to account for the differences in the thickness of sediments below different stations. The shallow structure (<0.7 km) was further confirmed by studying the arrival times for PS and SP converted phases on three component stations. Small offsets in the basalt layer (<50 m) below the faults (Paper 2) do not contribute any significant errors in the locations. The Vp/Vs ratio used for the lower layers was found to yield the lowest RMS residual values in the earthquake locations. The velocity model was tested by locating blasts used in the refraction surveys. The epicenters were located within 870, 555 and 385 m of the actual sites (Talwani, 1982). Thus, the "absolute" locations obtained by using HYPOELLIPSE are considered to be robust and reliable. Of these, 217 earthquakes were located with quality A and B, with a mean RMS residual of 0.08 s. These correspond to horizontal and vertical location errors of <1.3 km and <2.0 km respectively (Lahr, 1996). The epicenters of these quality A and B events are shown in Figure 3 together with the focal mechanisms of 17 of the well located events. This set of 17 well-constrained fault plane solutions with a strike uncertainty ≤ 15° were obtained by using FPFIT and FPPLOT (Reasenberg and Oppenheimer, 1985). The focal mechanisms indicate compressional deformation, in

agreement with the originally inferred direction of $S_{Hmax}$, N60ºE (Talwani, 1982; Zoback, 1983). To further improve the relative locations for tectonic interpretation, we input these 217 events in the double difference (DD) location algorithm HypoDD (Waldhauser, 2001).

The DD-technique can be applied when the hypocentral separation between two earthquakes is small compared to the distance to common stations and the scale length of velocity heterogeneity in the hypocentral region. In such case, the ray paths are similar and the differences in travel times are mainly due to the spatial offset between earthquakes.

P and S wave arrival data for 217 events were obtained from the 1974-2004 catalog and were used to obtain the travel-time differences for each event pair, with a separation distance less than 5 km at stations located within 200 km of the cluster centroid. To solve the forward problem, we used the 1D-layered P and S velocity model (Talwani, 1982) shown in Table 1. The HypoDD program that we used did not allow for different Vp/Vs ratios for different layers. Consequently a Vp/Vs ratio of 1.71 was used for all the layers (Table 1), in contrast to HYPOELLIPSE where a value of 2.93 was used for the top layer. At the end of the iteration process, a total of 148 events were relocated by HypoDD. The relocated events were grouped into 3 clusters, the first group consisting of 144 events and the other two consisting of two events each. For the first cluster, we observed a reduction of the average RMS residual from 0.09 s. to 0.02 s and was used for tectonic intrepretation. The other clusters contained too few events to yield a meaningful tectonic interpretation. Summarizing, only 144 events from a total of 217 events (66%) in the 1974-2004 catalog were captured by HypoDD with an average RMS residual of 0.02 s. Many of the events rejected by HypoDD because of poor station coverage outside the main cluster had reliable hypocentral HYPOELLIPSE locations. They were, therefore, later used in our analysis to define structures outside the main cluster.

HypoDD is a relative relocation program that is useful in defining seismogenic structures in 3D. However, it is not nearly as accurate at determining the absolute locations (Waldhauser and Richards, 2004) (Figure 4). Therefore, it was considered necessary to use additional data, for example, well determined hypocenters of larger events, geological, geophysical and geomorphological data, etc., to constrain the absolute locations (Waldhauser and Richards, 2004).

To estimate the expected epicentral displacement of hypocenters (given by HypoDD) with respect to their absolute locations (given by HYPOELLIPSE), we compare these two kind of locations, for 27 earthquakes of magnitude $\geq 2.5$. All these earthquakes were well located by HYPOELLIPSE with RMS $\leq 0.08$ s. We found that 23 out of 27 epicenters were displaced with HypoDD less than 2 km from their HYPOELLIPSE location with an average epicentral displacement of about 1.4 km to the southeast (Figure 5 and Table 2). The systematic SE displacement could possibly be because of the incorrect Vp/Vs ratio used for the top layer in HypoDD and the paucity of stations to the northwest of the epicentral area (Figure 6). We also calculated the change in their hypocentral depths and found no systematic changes. For 21 of the 27 events the changes in depth ranged between -2.0 and +0.9 km. The largest changes in depths were -3.1 km and 4.3 km. Only the systematic epicentral displacement to the southeast was considered in our seismotectonic interpretation described later in this paper.

**5. Discrimination**

The revised epicentral locations (Figure 4) do not outline any obvious fault trends, but the various fault plane solutions (Figure 3) suggest that both thrust and strike-slip faults are active in this area. In particular, we note the existence of fault planes oriented primarily NW-SE associated with reverse motion, and also of fault planes oriented N-S associated

with both right-lateral strike-slip and reverse motion. From the epicentral locations alone it was not obvious which nodal plane (for the various fault plane solutions) was the fault plane. Therefore, we divided these fault plane solutions into two groups: group I associated with predominantly NW-SE trending faults and group II associated with N-S trending fault planes (Tables 3a and 3b).

In order to separate the hypocenters into the different groups we took the following approach. We reasoned that movements on different faults would be associated with different first motions on one or more optimally located seismic stations. To distinguish which earthquakes belonged to which fault planes, we examined the first motions for each earthquake at stations of the SCSN. This was in a search for systematic polarity differences at any station for earthquakes associated with different faults in the same hypocentral region.

Figure 6a shows the locations of the seismic stations which surround the observed seismicity. We considered reliable first-motion data (only picks with a weight of 0 or 1, in computer program HYPOELLIPSE) for all earthquakes at all recording stations. Figure 6a shows an outline of the seismically active area (oval) and the locations of the seismic stations. Figure 6b shows a histogram of the numbers of events with compressional and dilatational first arrivals by station for all earthquakes listed in the HypoDD catalog. Note that stations BCS (surface sensor), CSU (surface sensor) and CSB (borehole sensor) are essentially at the same location; BCS was moved about 1 km to CSU in 1998. We grouped the arrivals at BCS and CSU (both surface sensors) and denote them as ΣCSU. The number of arrivals at NHS, SGS and HWD were considered to be too few to use as discriminants.

To decide which station(s) to use as discriminants, as a first step we analyzed the first-motion data for a set of 17 earthquakes with well-constrained fault plane solutions, which were divided into two groups depending on the inferred strike of their fault planes

(Tables 3a and 3b). Our selection of the fault planes was based on the number of solutions along those planes and our current understanding of the seismotectonics of the MPSSZ area (Durá-Gómez, 2004) (Figure 2). For convenience in the analysis, the compressional and dilatational first arrivals were assigned a numerical value of 1 and 2, respectively. Then, for each station in each group of earthquakes, we calculated the average of the assigned values. For example, for station RGR there were nine events in group I of which 5 were compressional (designated value 1) and four were dilatational (designated value 2) for an average designated value of 1.4. However, for ΣCSU (sum of CSU and BCS), there were 10 events with an average designated value of 1.9 i.e. predominantly dilatational. Similarly the average designated values were obtained for group II (Table 3b). Then these 'average designated value' for a particular station was compared for each of the two groups (Table 3c). If the difference between the average designated values was greater than 0.5 it was used as a diagnostic. Two stations, WAS and ΣCSU, met this criterion. We considered station ΣCSU (sum of CSU and BCS, Figure 8) as our diagnostic station based on the fact that 16 earthquakes were used in obtaining the average value, while only 12 earthquakes were used in the case of WAS. Therefore, we concluded that earthquakes associated with group I (predominantly on NW striking faults) had usually dilatational first arrivals at ΣCSU (average value of 1.9; Table 3a), while earthquakes associated with group II (on N-S oriented faults) had mostly compressional first arrivals at ΣCSU (average value of 1.3; Table 3b). So while examining all other earthquakes, as the first step, we used the above criterion to separate the cluster of earthquakes in the MPSSZ into two bins – dilatational first arrivals at ΣCSU which we associated with reverse movement on NW trending faults and compressional first arrivals which we associated with strike-slip on NNE-SSW and N-S trending faults.

We noted that the depths of all the well located events (using HypoDD) were between 3 and 16 km (Figure 7). Drilling at Clubhouse Crossroads (Figure 6a) encountered basalt flows at a depth of ~0.7 km (Gohn et al., 1983), below the pre-Cretaceous unconformity (Ackermann, 1983). The three wells at Clubhouse Crossroads were abandoned only a few meters into the basalt and did not penetrate the entire sequence of basalt flows. However a speculative well (in search of oil and gas) drilled at Lodge (33º 00' 54" North, 80º 55' 44" West) encountered basalt at depth of 1.4 km. It was drilled to a total depth of 3.8 km and bottomed out in basalt (Talwani, 2000, unpublished data) suggesting that the basalt extended to a greater depth. The crystalline basement lies below the layer of basalt flows and intercalated sediments. In the MPSSZ, based on the seismic refraction velocities, Ackermann (1983) interpreted the top of the crystalline basement to be located between 1200 m and 2400 m. We interpret the hypocentral depths at MPSSZ ($\geq$ 3 km) to suggest that the earthquakes are occurring along faults below the basalt and in the crystalline basement.

Figure 8 shows the epicentral locations of events located by HypoDD, segregated by their first arrivals at ΣCSU. Since HypoDD locations did not include epicenters north of Summerville because of inadequate station coverage to the north, we included well located events (HYPOELLIPSE) in that area (stars) for which the first arrival was primarily compressional to better identify the WF. Note that the relative epicentral locations obtained by HypoDD are offset ~1.4 km to the southeast compared to those obtained by HYPOELLIPSE (stars). For tectonic interpretation, the relative locations obtained from HypoDD were moved 1.4 km to the northwest and merged with the absolute locations from HYPOELLIPSE. We note that the most intense seismicity occurs in the vicinity of Fort Dorchester and Middleton Place. In this area epicenters with both dilatational and

compressional first arrivals at ΣCSU are present, suggesting the presence of two or more styles of faulting, although dilatational arrivals are predominant. To the north of Fort Dorchester, the seismicity is less dense, however epicenters with both compressional and dilatational first arrivals at ΣCSU are present (Figure 13).

We plotted these earthquakes in cross-sections to study their three-dimensional configuration. The hypocenters were viewed in 3-D using the ArcScene visualization tool of ArcGIS (ESRI Inc., 2007). The directions of the cross sections were chosen based on the 3-D configuration of the hypocenters and other supporting geomorphophic and/or geophysical data. All earthquakes with dilatational first arrivals at ΣCSU (solid circles, Figure 8) were plotted along a cross-section AB consistent with the 3-dimensional views of hypocenters (Figure 9), drawn perpendicular to Dorchester Creek (DC in Figure 8). The location of the Dorchester Creek was inferred to be fault controlled based on its geomorphic configuration. In this cross-section, we notice two clusters of seismicity separated by about 5 km along with a few outliers. Most of the epicenters in the southwestern cluster (shown in red in Figure 9) lie within ~2.5 km of Dorchester Creek and its SE extension up to Middleton Place, at depths of about 3 km and 13 km, and define a broad zone of seismicity. We have named it the Sawmill Branch fault zone (SBFZ) because of the overlying Sawmill Branch – Dorchester Creek (DC in Figure 8). We interpret the configuration of the SBFZ seismicity in two different but possible ways. The first is a broad zone dipping about 70º to the SW (Figure 9a), the second is a series of parallel faults dipping steeply to the NE (Figure 9b). Of these two interpretations we prefer the latter based on mechanical arguments that are described in the next section. The northeastern cluster (shown in blue in Figure 9) defines a narrow SW dipping zone with depths between ~6 km and 12 km. If this zone is extended to the surface, it lies roughly near the surface location of the NW-SE trending Charleston fault

(CF), mapped by shallow drilling (Colquhoun et al., 1983; Lennon, 1985; Weems and Lewis, 2002) (Figure 9a). The hypocenters are inadequate to accurately constrain the dip of CF. Using shallow stratigraphic data that defined the presence of Mt. Holly dome (Weems and Lewis, 2002) (Paper 2), we estimate a dip of about 40º for CF.

We plotted all the earthquakes located by HypoDD with compressional first arrivals at ΣCSU (Figure 8) along a cross-section CD. Seismic reflection surveys (Hamilton et al., 1983; Marple, 1994) had mapped a NE trending fault in the basalt layer at a depth of 700 m under the Coastal Plain sediments. This fault was identified as Woodstock fault (North) (Durá-Gómez, 2004) and cross-section CD, trending N60ºW to S60ºE, was chosen perpendicular to this Woodstock fault (Figure 10). We note that the hypocenters define a NW dipping plane.

A number of earthquakes in the Summerville area (northern area of MPSSZ) were not included in the final solution given by HypoDD due to the poorer station coverage of these events. Because they were well located (quality A and B solutions using HYPOELLIPSE), they are included here in our tectonic evaluations. These ten events, with compressional first arrivals at ΣCSU, are shown by stars in Figure 8. We note that the epicenters of the earthquakes with compressional first arrivals at ΣCSU lie in two broad zones: one to the north of Fort Dorchester and the other to its southeast. These additional ten events were added to the cross section along CD and are shown by squares in Figure 11a. In this cross section, to compare with the absolute locations obtained from HYPOELLIPSE, the relative locations obtained from HypoDD were moved 1.4 km (see Table 2) to the NW (Figure 11a). Of these 10 events, four, shown by green squares seem to define an additional plane dipping to the NW, whereas the other six, shown by pink squares lie to the northwest. The epicentral locations of the events comprising the NW dipping

planes are shown in Figure 13. Those epicenters that lie to the N of the Ashley river and have been associated with WF(N) are shown in green in both Figures 11a and 13. Another set of hypocenters (shown in yellow in Figures 11a and 13) lying to the SE of WF(N) outline Woodstock fault South, WF(S). The two are offset ~6 km at the surface, and converge at depth. These data, suggest a northwestern dip of about 50º for WF(S), and a steeper dip for WF(N).

Northwest and southeast of the line marked EF in Figure 8, we note a broad NW-SE trend of epicenters with compressional first arrivals at ΣCSU (open dots in Figure 8). This trend is also apparent in the original locations obtained by using HYPOELLIPSE (Figure 3). We interpret these observations to suggest the possible existence of another NW-SE trending fault plane. However, seven of these earthquakes, including three events well located by HYPOELLIPSE but not located by HypoDD, were used earlier in defining Woodstock-north, and are shown by green dots in Figure 13. Removal of these events from the cross-section along CD (Figure 11b) and including them instead in a cross-section along EF (Figure 12a) suggest the presence of a steep (~80º) NE dipping fault, which we have named the Lincolnville fault (LF in Figure 13). However, if we retain these events in Figure 11a, the few remaining hypocenters in a cross-section along EF (Figure 12b) are inadequate to clearly define any fault plane. Nevertheless the 3-D view suggests that they are possibly associated with two NE dipping planes. So we note that while Figure 11a and 12b support the presence of WF(N), Figures 12a and 11b suggest the presence of LF. The seismicity data alone cannot distinguish between these interpretations or rule out the presence of both faults. To distinguish between these possibilities we had to incorporate additional geological and geophysical data (Paper 2).

Our revised tectonic framework in the Middleton Place Summerville area is shown in Figure 13. The epicenters are shown in the same colors as in the cross sections (Figures 9-12). We combined the dips obtained from the cross sections with other data to project the faults to the surface. For the WF(N) we took its location at a depth of ~700m, inferred from the seismic reflection data, and a dip of ~50º to obtain its location at the surface. We took the surface projection of the seismicity (Figure 9b) to define the SBFZ. We used the linear portion of the Dorchester Creek (from ~32º 57.926' N, 80º 10.6625'W) and extending SE along the Ashley River to Middleton Place to represent the surface expression of the main segment of the SBFZ, and to define its lateral extent. For the strike and extent of the WF(S), we followed the configuration given by Durá-Gómez (2004). That was based on the 3-D configuration of the seismicity near Middleton Place and to its SW up to the Adams Run Seismic Zone and on the location of the M3.4 earthquake on October 23, 1967 by Dewey (1983) (Figure 2). This configuration is supported by a variety of other data which are described in Paper 2. For the CF and LF we took their surface locations from surface projections of the seismicity shown in the cross sections of Figures 9b and 12a. The aseismic ARF, which lies along the Ashley River between Middleton Place and the Magnolia Plantation, lies outside the seismotectonic framework containing the faults associated with the current seismicity. Based on the focal mechanisms (Talwani, 1982; Madabhushi and Talwani, 1993; Garner, 1998; Durá-Gómez, 2004; and this study), and the WF(N and S) faults are associated with right–lateral oblique-strike-slip motion, while the NW-SE trending faults, steeply dipping in the SBFZ and LF and shallowly dipping CF, are associated with oblique left-lateral strike-slip and reverse faulting in response to an in-situ stress field with the direction of the maximum horizontal stress field oriented N60ºE (Figure 13).

## 6. Conclusions

Macroscopic observations following the 1886 Charleston earthquake, and analysis of seismicity data between 1974 and 2004 (e.g. Talwani, 1982; Madabhushi and Talwani, 1993; Garner, 1998; Talwani, 2001; and Durá-Gómez, 2004) suggest that there are two or more active fault planes in the Middleton Place Summerville Seismic Zone undergoing compressional deformation in response to a stress field with the direction of the maximum horizontal stress ($S_{Hmax}$) oriented ~N60ºE. We used the polarity of the first arrivals at ΣCSU and suitably oriented cross-sections using revised hypocenters obtained by HypoDD, to obtain a revised seismotectonic framework and identify the fault planes on which the seismicity is occurring. The results of these studies suggested the presence of a major NE-SW strike-slip fault system (WF), with NW-SE trending thrust fault(s) near Middleton Place. The geometry and the nature of these faults were not previously well defined.

The revised framework consists of the N30ºE oriented, Woodstock fault (WF) associated with oblique right-lateral strike-slip motion, which because of its length was probably associated with the mainshock of the 1886 Charleston earthquake. WF has an antidilatational compressional left step near Middleton Place, which divides it into two parts, WF(N) and WF(S), both of which dip steeply (≥50º) to the NW. The seismicity along these faults lies between depths of 3 and 12 km. WF(N) and WF(S) are separated by ~6km at the surface (at the left step) and converge at depth. Most of the current microearthquake activity is occurring along three roughly parallel, N30ºW to N40ºW striking faults located within the left step. These NW-SE striking faults are oriented at about ~60º to 70º to WF. The most active of these is the ~3 to 4 km broad, diffuse, Sawmill Branch fault zone (SBFZ) which offsets the WF near Middleton Place. About 5 km and 18 km northeast of SBFZ lie the Lincolnville and Charleston faults (LF and CF), respectively. LF dips steeply to the northeast

whereas CF dips shallowly to the southwest, and seismicity on these faults lies between depths of 3 and 12 km. Fault plane solutions for events in the SBFZ suggest reverse faulting on SW or NE dipping fault planes (events 3, 5 and 6 in Figure 3) or reverse faulting with left-lateral strike-slip motion on them (events 1, 2, 7 and 9 in Figure 3).

Our analysis using new and improved relocations using HypoDD suggest two possible geometric configurations for the broad SBFZ. The first is a broad SW dipping fault plane (Figure 9a), and the second, is a diffuse zone consisting of subparallel steep NE dipping faults, which together comprise the SBFZ (Figure 9b). We favor the latter interpretation which together with the NE dip of the LF and SW dip of the CF (Figure 14) is compatible with sand box models of restraining step-overs in strike-slip fault systems (McClay and Bonora, 2001), with the theoretical analysis by Segall and Pollard (1980) and with the analysis of antidilational jogs by Sibson (1986). Segall and Pollard (1980) suggested that, for left-stepping cracks, the mean stress is everywhere compressive and that the compression increases above the background value in the region between the cracks, while in the region outside the cracks the mean stress is less than the background value. For a driving stress increased above the frictional resistance to slip, left-lateral secondary shear fractures may form within the step oriented at about 60º to the lengthened segments (Segall and Pollard, 1980). In our case, the SBF, LF and CF lie at angles of about 60º to 70º to WF(N) and WF(S). Additionally, fault plane solutions suggest that the SBF behaves as a left-lateral fracture but also displays a significant reverse component.

The revised tectonic framework for the MPSSZ proposed in this paper is different from earlier interpretations in the following ways: (a) The seismicity in the MPSSZ is associated with a major strike-slip fault system (WF(S) and (N)) with an antidilational left step at Middleton Place. Three short NW-SE trending faults lie within this left step and,

together with WF(N) and (S), are the location of a localized stressed volume and the observed seismicity. This interpretation differs from our earlier interpretation where the seismicity was associated with fault intersections. (b) The inferred dip direction of the SBF (NE) is opposite to the earlier interpretation of a SW dip for it (Durá-Gómez, 2004) and the Ashley River fault (Talwani, 1982; Madhabhushi and Talwani, 1993; Garner, 1998). (c) The ARF, originally interpreted as a NW trending fault, extending from the Magnolia Plantation to Summerville, is now interpreted to be two faults. They are the seismically active SBF, lying within the step over and trending N30ºW from Middleton Place, and the aseismic ARF, trending ~S55ºE from Middleton Place to the Magnolia Plantation.

We compare our seismotectonic model with the analysis by Sibson (1986) and the seismicity pattern following the 1968 Borrego Mountain earthquake (Figure 15). In Sibson's analysis, the left stepping antidilational jog (Figure 15b) forms potential locking points, and slip transfer is accompanied by widespread subsidiary faulting. This faulting located in the left step consists of roughly parallel reverse faults that face each other (Figure 15b). He also found that seismicity was not confined within the left step but also occurred outside it. In our case, the MPSSZ (Figure 15a) mimics the seismicity pattern suggested by Sibson (1986). If we consider the SBFZ to consist of parallel NE dipping faults (Figure 9b) and with the CF dipping to the SW, the patterns and dips of the reverse faults observed within the left step closely resembles those suggested by Sibson (1986) (Figure 15b).

This pattern of strike-slip faulting on a main fault near a left step antidilational jog followed by reverse faulting on faults within the jog was observed in the M6.4 1968 Borrego Mountain earthquake sequence (Figure 15c). The main-shock was associated with right-lateral strike-slip on a NW striking fault plane and was followed by a left-lateral strike-slip event on the main fault a reverse faulting on the cross faults within the left-step (Burdick and

Mellman, 1976). Our seismotectonic framework for MPSSZ is compatible with the results from sand box experiments (McClay and Bonora, 2001) and with the analysis of antidilational jogs by Sibson (1986) and with the faulting observed in the Borrego Mountain earthquake sequence.

In the seismotectonic framework presented in this paper, we note that the seismicity in MPSSZ occurs along different faults and by different mechanisms. These faults lie deeper than ~3km, i.e., below the Coastal Plain sediments and the extensive basalt flows. Movements on these faults affected the overlying basalt flows and sediments, and they accounted for the different macroscopic effects described earlier in this paper. Both the sand box experiments (McClay and Bonora, 2001) and Sibson's (1986) analysis predict localized uplift between the SBFZ and CF.

To test the validity of our model of the seismotectonic framework, we compare these locations of the faults and inferred movements on them with a variety of complementary data in the companion paper (Talwani and Durá-Gómez, 2009).

**7. Data and Resources**

All data used in this paper came from published sources listed in the references.

**8. Acknowledgments**

We thank Profs. Jim Knapp, Tom Owens and Dr. G. Lin for their suggestions to improve the quality of the manuscript. We are specially appreciative and grateful to Prof. John Ebel for his detailed review. We also thank Martin Chapman for his insightful comments. The study was supported by grants from the Savannah River Site and the U.S. Geological Survey.

**9. References**

Ackermann H. D. (1983). Seismic-refraction study in the area of the Charleston, South Carolina, 1886 earthquake, in *Studies Related to the Charleston, South Carolina, Earthquake*

*of 1886 – Tectonics and Seismicity*, G. S. *Gohn (Editor), U.S. Geological Survey Professional Paper 1313,* F1-F20.

ArcGIS (ESRI Inc. 2007). www.esri.com/arcgis

Bakun, W.H. and M.G. Hopper (2004). Magnitudes and locations of the 1811-1812 New Madrid, Missouri, and the 1886 Charleston, South Carolina, Earthquakes, *Bull. Seism. Soc. Am.* **94**, 64-75.

Bollinger, G. A. (1977). Reinterpretation of the Intensity Data for the 1886 Charleston, South Carolina, Earthquake, in *Studies related to the Charleston, South Carolina, earthquake of 1886; a preliminary report, D. W. Rankin (Editor), U.S. Geological Survey Professional Paper 1028,* 17-32.

Bollinger, G. A. (1983). Speculations on the nature of seismicity at Charleston, South Carolina. U. S, in *Studies Related to the Charleston, South Carolina, Earthquake of 1886 – Tectonics and Seismicity*, G. S. *Gohn (Editor), U.S. Geological Survey Professional Paper 1313,* T1-T11.

Burdick, L. J. and G. R. Mellman (1976). Inversion of the body waves from the Borrego Mountain earthquake to the source mechanism, *Bull. Seism. Soc. Am.* **66**, 1485-1499.

Burford, R. O. (1968). Continued slip on the Coyote Creek fault after the Borrego Mountain earthquake, in *The Borrego Mountain earthquake of April 9, 1968*, *U.S. Geological Survey Professional Paper 787,* 105-111.

Colquhoun, D. J., I. D. Woollen, D. S. Van Nieuwenhuise, G. G. Padgett, R. W. Oldham, D. C. Boylan, P. D. Howell and J. W. Bishop (1983), Surface and subsurface stratigraphy, structure and aquifers of the South Carolina Coastal Plain, *Columbia, State of South Carolina, Office of the Governor, Ground Water Protection Division, Report for Department of Health and Environmental Control,* 78 pp.

Dewey, J. (1983). Relocation of instrumentally recorded pre-1974 earthquakes in the South Carolina region, in *Studies Related to the Charleston, South Carolina, Earthquake of 1886 – Tectonics and Seismicity*, G. S. *Gohn (Editor), U.S. Geological Survey Professional Paper 1313,* Q1-Q9.

Durá-Gómez, I. (2004). Seismotectonic framework of the Middleton Place Summerville Seismic Zone near Charleston, South Carolina, *M.S. Thesis*, Columbia, University of South Carolina, 194 pp.

Dutton, C. E. (1890). The Charleston Earthquake of August 31, 1886, *U.S. Geological Survey Annual Report, Report: 9, 203-528 ( Republished in 1975).*

Ellsworth, W. L. (1977). Three-dimensional structure of the crust and mantle beneath the island of Hawaii, *Ph. D thesis*, Massachusetts Institute of Technology, Cambridge, 327pp.

Garner, J.T. (1998). Re-evaluation of the Seismotectonics of the Charleston, South Carolina Area, *M.S. Thesis*, Columbia, University of South Carolina, 250 pp.

Gohn G. S., B. Houser and R. R. Schneider (1983). Geology of the lower Mesozoic(?) sedimentary rocks in Clubhouse Crossroads test hole #3, near Charleston, South Carolina, in *Studies Related to the Charleston, South Carolina, Earthquake of 1886 – Tectonics and Seismicity*, G. S. *Gohn (Editor), U.S. Geological Survey Professional Paper 1313,* D1-D17.

Hamilton, R.M, J.C. Behrendt and H.D. Ackermann (1983). Land multichannel seismic reflection evidence for tectonic features near Charleston, South Carolina, in *Studies Related to the Charleston, South Carolina, Earthquake of 1886 – Tectonics and Seismicity*, G. S. Gohn (Editor), *U.S. Geological Survey Professional Paper 1313,* I1-I18.

Johnston, A.C. (1996). Seismic moment assessment of earthquakes in stable continental regions, III. New Madrid 1811-1812, Charleston and Lisbon 1755, *Geophys. J. Int.* **126**, 314-344.

Lahr, J. C. (1996). Quick-start manual for HYPOELLIPSE Version 3.0., A Computer Progam for Determining Local Earthquake Hypocentral Parameters, Magnitude, and First-Motion Pattern, *U.S. Geological Survey.*

Lennon, G. (1985) Identification of a northwest trending seismogenic graben near Charleston, *M.S. Thesis*, Columbia, University of South Carolina, 84 pp.

Louderback, G.L. (1943). The personal record of Ada M. Trotter of certain aftershocks of the Charleston earthquake of 1886, *Bull. Seism. Soc. Am.* **33**, 199-206.

Madabhushi, S. and P. Talwani (1983). Fault plane solutions and relocations of recent earthquakes in Middleton Place Summerville Seismic Zone near Charleston, South Carolina, *Bull. Seism. Soc. Am.* **83**, 1442-1466.

Marple, R. T. (1994). Discovery of a possible seismogenic fault system beneath the Coastal Plain of South and North Carolina from integration of river morphology and geological and geophysical data, *Ph.D. Thesis*, Columbia, University of South Carolina, 354 pp.

McClay,K. and M. Bonora (2001). Analog models of restraining stopovers in strike-slip fault systems, *AAPG Bull.* **85**, 233-260.

McKinley, C. (1887). A descriptive narrative of the earthquake of August 31, 1886, in *Appendix for the City (of Charleston) Year Book, 1886,* 345-441.

Reasenberg, P. A., and D. Oppenheimer (1985). FPFIT, FPPLOT, and FPPAGE: Fortran computer programs for calculating and displaying earthquake fault-plane solutions, *U.S. Geol. Surv. Open-File Rept. 85-0739.*

Segall, P. and D. D. Pollard (1980). Mechanics of discontinuous faults, *J. Geophys. Res.* **85**, 4337-4350.

Shedlock, K.M. (1987). Earthquakes recorded by the South Carolina Seismic Network, *U.S. Geol. Surv. Open-File Rept. 87-0437.*

Shedlock, K. M. (1988). Seismicity in South Carolina, Seismological Research Letters, **59**, 165-171.

Sibson, R.H., 1986. Rupture interaction with fault jogs, in *Earthquake Source Mechanics*, eds Das, S., Boatwright, J. & Scholz, C.H., *AGU Geophysical. Monograph.*, **37**, *Maurice Ewing Ser. 6*, 157–167.

Taber, S. (1914). Seismic Activity in the Atlantic Coastal Plain near Charleston, South Carolina, *Bull. Seism. Soc. Am.*, **4**, 108-160.

Talwani, P. (1982). Internally consistent pattern of seismicity near Charleston, South Carolina, *Geology*, **10**, 654-658.

Talwani, P. (2000). Velocity structure inferred from an exploratory oil well in Colleton County, South Carolina. Unpublished report, 4pp.

Talwani, P., (2001). Macroscopic effects of the Charleston earthquake, *73rd Annual Meeting of the Eastern Section of the Seismological Society of America,* Field Trip Guide, October 14, 2001.

Talwani, P., and I, Durá-Gómez, (2009). Finding faults in the Charleston Area, South Carolina: 2. Complementary data. Submitted to Seis. Res. Lett.

Tarr, C., P. Talwani, S. Rhea, D. Carver and D. Amick (1981). Results of recent South Carolina seismological studies, *Bull. Seism. Soc. Am.* **71**, 1883-1902.

Tarr C. and S. Rhea (1983). Seismicity near Charleston, South Carolina, March 1973 to December 1979. U. S., in *Studies Related to the Charleston, South Carolina, Earthquake of*

*1886 – Tectonics and Seismicity*, G. S. *Gohn G. S. (Editor), U.S. Geological Survey Professional Paper 1313,* R1-R17.

Waldhauser, F. (2001). HypoDD: a program to compute double-difference hypocenter locations, *U.S. Geol. Surv. Open-File Rept. 01-113*.

Waldhauser, F. and W. L. Ellsworth (2000). A double-difference earthquake location algorithm: Method and application to the northern Hayward fault, California, *Bull. Seism. Soc. Am.* **90**, 1353-1368.

Waldhauser, F. and P.G. Richards (2004). Reference Events for Regional Seismic Phases at IMS Stations in China, *Bull. Seism. Soc. Am*., **94**, 2265–2279.

Weems, R. E. and W.C. Lewis (2002). Structural and tectonic setting of the Charleston, South Carolina, region: Evidence from the Tertiary stratigraphy record, *GSA Bulletin*, **114**, 24-42.

Zoback, M.D. (1983). Intraplate earthquakes, crustal deformation, and in-situ stress, in *A workshop on "The 1886 Charleston, South Carolina, earthquake and its implications for today", W. W. Hays and P. L. Gori (Editors), U.S. Geol. Surv. Open-File Rept. 83-843*, 169-178.

**Authors' affiliations**

Department of Geological Sciences

University of South Carolina

701 Sumter Street

Columbia, SC 29208

**List of figures**

Figure 1: The three foci of the 1886 Charleston earthquake (Woodstock, Middleton Place and Ratowles) according to Sloan (in McKinley, 1887). Taber's inferred fault (Taber, 1914) for that earthquake is shown with a bold line.

Figure 2: Epicentral locations (cream color circles) showing A and B quality microearthquakes between 1974 and 2004 and fault plane solutions of the 08/21/1992 M 4.1 and the 07/22/2001 M 2.3 earthquakes. The dense cluster of seismicity surrounding Fort Dorchester has been named the Middleton Place Summerville Seismic Zone (Tarr et al., 1981). The blue dot shows the location of the October 23, 1967, M3.4 earthquake (Dewey, 1983). The red bold lines show the seismotectonic framework according to Durá-Gómez (2004). The framework consists of the NE trending Woodstock fault (WF) which is cut and offset to the NW along the Sawmill Branch fault (SBF).

Figure 3: Seismicity for the period 1974 to 2004 (quality A and B solutions using HYPOELLIPSE) and 17 well-constrained fault plane solutions (the strike directions are good to $\leq 15^{o}$). All solutions suggest compressional deformation with $S_{Hmax}$ oriented N60ºE (open arrows). Solutions 1-10 are predominantly associated with NW-SE trending reverse faults; and 11-17 with N-S trending strike-slip and reverse faults. Squares and circles with a dot show locations of towns and important landmarks. The epicenters located in the southwest corner define the Adams Run Seismic zone of Tarr et al. (1981). The location of the 1967 earthquake was obtained from Dewey (1983).

Figure 4: Relocated epicentral locations using HypoDD. Note that only about two thirds of the epicenters shown in Figure 3 could be relocated using this method.

Figure 5: Rose diagram showing the angle of displacement from HYPOELLIPSE to HypoDD epicentral locations (measured from the north). The radii give the number of events.

Figure 6a: Location of seismic stations and boundary of main seismicity area. SGS is located (33.1925ºN, 80.5095ºW) outside the figure. NHS, TWB and HWD were deactivated in 1980, 2006 and 1995 respectively. CCC1 shows the location of Clubhouse Crossroads well # 1. DC shows the location of Dorchester Creek, its NE continuation is called Sawmill Branch.

Figure 6b: Numbers of compressional and dilatational first arrivals by station for all earthquakes located by HypoDD. ΣCSU is the sum of CSU and BCS.

Figure 7: Depth distribution of earthquakes (using HypoDD). Most of the hypocenters lie between 3 and 13 km depth.

Figure 8: Epicentral locations obtained from HypoDD. Earthquakes with compressional and dilatational first arrivals at ΣCSU are shown by open and solid circles, respectively. A and B quality locations of events obtained by HYPOELLIPSE north of the Summerville scarp are shown by stars. DC shows the location of Dorchester Creek. Cross-sections were obtained along AB, CD and EF (see text for details).

Figure 9a: Cross-section along AB (Figure 8) oriented S60ºW–N60ºE showing earthquakes with dilatational first arrivals at ΣCSU (solid circles in Figure 8), that define the Sawmill Branch fault zone (SBFZ) and the Charleston fault (CF). The shaded area in red shows the interpreted location of basalt flows and intercalated sediments. A preliminary interpretation suggests a ~70° SW dip for SBFZ and a ~40° SW dip for CF. DC (blue square) on the surface shows the location of Dorchester Creek. CD shows where the cross-section along CD intersects the present cross-section.

Figure 9b: An alternate interpretation of the cross-section along AB suggests the presence of a series of parallel faults in the SBFZ dipping steeply to the NE, while the CF dips ~40° to the SW. The shaded area in red shows the interpreted location of basalt flows

and intercalated sediments. DC (blue square) on the surface shows the location of the Dorchester Creek. CD shows where the cross-section along CD intersects the present cross-section.

Figure 10: Cross-section along CD (Figure 8) oriented N60ºW-S60ºE, showing only compressional arrivals at ΣCSU (open circles in Figure 8). The shaded area is the inferred location of basalt flows and intercalated sediments. AB shows where the cross-section along AB intersects the present cross-section.

Figure 11a: Cross-section along CD (Figure 8) showing earthquakes with compressional first arrival at ΣCSU. Earthquakes located by using HypoDD, and A and B quality hypocentral locations obtained with HYPOELLIPSE are shown by triangles and squares respectively. The colors are coordinated with their epicentral locations shown in Figure 13. Earthquakes associated with WF(N), green, lie to the N and W of the Ashley River, whereas those with WF(S), yellow, lie along the Ashley River and to its south. Earthquakes located using HypoDD have been translated 1.4 km to the NW to compare with the absolute locations given by HYPOELLIPSE and supplementary data. The shaded area shows the interpreted location of basalt flows and intercalated sediments. The faults mapped in the basalt are shown as blue triangles. This and other complementary data suggest that the surface expression of the WF(S) is located at ~ (0, 0) km while the surface expression of WF(N) is located at ~ (6.3, 0) km. WF(S) dips about 50º to the NW. The inferred location of both WF(S) and WF(N) at the surface is in agreement with corroborative data on the basalt flows (700 m depth) and surface geology (see companion paper). The dip of WF(N) is not well constrained. AB shows where the cross-section along AB intersects the present cross-section.

Figure 11b: Resulting cross-section along EF after the removal of the seven earthquakes in Figure 11a which are included Figure 12a (in green) to define the LF.

Figure 12a: Cross-section along EF (map view in Figure 8 and shown in gray and green in Figure 13). Earthquakes that were used to interpret the WF(N) (Figure 11a) are shown in green. Hypocentral locations suggest a steep (~80º) NE dipping fault, which we have named the Lincolnville fault (LF). The shaded area shows the interpreted location of basalt flows and intercalated sediments.

Figure 12b: Cross-section along EF (map view in Figure 8 and shown in green in Figure 13). The earthquakes that were used to describe the WF(N) in Figure 11a have been removed. The remaining hypocentral locations are too few to define a fault plane(s). The shaded area shows the interpreted location of basalt flows and intercalated sediments.

Figure 13: Close up view of the revised seismotectonic framework based on the analysis of seismological data showing the inferred faults and the earthquakes used to define them. The epicentral locations of the earthquakes are color-coordinated with the different faults interpreted here, and in the cross sections (Figures 9-12). They are WF(S) (yellow), WF(N) (green), SBF (red), CF (blue), and LF fault (gray). For the epicenters shown in red and blue the first arrival at CSU was down and for those shown in gray, green and yellow, it was up. Open arrows show the $S_{Hmax}$ direction, N60ºE. The figure shows the most prominent styles of faulting.

Figure 14: The revised seismotectonic framework. WF(N) continues NE to Pinopolis, and WF(S) continues SW to the Adams Run Seismic Zone near a town by that name.

Figure 15: Comparison of the (a) seismotectonic framework of the MPSSZ with (b) the analysis of Sibson (1986) for antidilational jogs and (c) the style of faulting of the 1968

Borrego mountain earthquake and its aftershocks, modified from Burford (1968) and Burdick and Mellman (1976). The ellipse in (a) shows the boundary of the MPSSZ seismogenic area. In antidilational jogs Sibson reports compression associated with folds and thrusts, as well as large aftershock distributions (shaded area). Our interpretation of the seismotectonic framework for MPSSZ, a right-lateral strike-slip fault with a left-step associated with a series of steeply dipping reverse faults with opposing dips, agrees with the analysis of Sibson (1986) for the style of faults with an antidilational left-stepping jog. The style of faulting at Charleston, right-lateral on WF and (primarily) reverse on SBF, is similar to that observed from the Borrego Mountain earthquake.

**Table 1: Velocity model used for hypocenter determination***

| Vp (km/s) | Depth of top of layer (km) | Vp/Vs |
|---|---|---|
| 2.20 | 0.00 | 2.93 |
| 5.50 | 0.75 | 1.71 |
| 5.60 | 1.50 | 1.71 |
| 5.75 | 3.00 | 1.71 |
| 5.90 | 7.00 | 1.71 |
| 6.45 | 10.0 | 1.71 |
| 6.70 | 20.0 | 1.71 |
| 8.15 | 30.0 | 1.71 |

* The above model was used in the program HYPOELLIPSE. For use in HypoDD, a constant Vp/Vs ratio of 1.71 was used for all layers.

**Table 2:** Hypocentral changes of relocated earthquakes of magnitude ≥ 2.5 with respect to their absolute locations given by HYPOELLIPSE.

Earthquake (year/month/date/hour/min.)
M=Magnitude
D=Epicentral displacement from HYPOELLIPSE to HypoDD solution
Ang=Angle of displacement from HYPOELLIPSE to HypoDD epicentral locations (with respect to north)
Δ depth=Change in depth from HYPOELLIPSE to HypoDD epicentral locations (HYPODD-HYPOELLIPSE)

| **Earthquake** | **M** | **D (km)** | **Ang.** | **Δ depth (km)** |
|---|---|---|---|---|
| 197703300827 | 2.9 | 1.9 | 70º | -3.1 |
| 198801230157 | 3.1 | 1.3 | 210º | -1.7 |
| 198901021635 | 2.7 | 0.9 | 185º | -1.1 |
| 199002070741 | 2.8 | 1.6 | 250º | -1.8 |
| 199005111832 | 2.5 | 0.8 | 110º | 0.5 |
| 199006020257 | 2.5 | 1.4 | 150º | -0.7 |
| 199006181003 | 2.8 | 1.5 | 140º | -0.7 |
| 199011131522 | 3.3 | 0.8 | 200º | 0.2 |
| 199108182246 | 2.9 | 1.7 | 190º | -1.7 |
| 199205072011 | 2.5 | 1.0 | 70º | 3.3 |
| 199208211631 | 4.0 | 1.5 | 150º | 0.9 |
| 199504171346 | 3.4 | 1.2 | 140º | 2.5 |
| 199711260520 | 2.5 | 1.4 | 170º | 0.0 |
| 199903291449 | 3.0 | 1.4 | 110º | 3.5 |
| 200112230557 | 2.8 | 1.5 | 130º | -1.5 |
| 200201111330 | 2.7 | 2.6 | 140º | 0.8 |
| 200207070240 | 2.9 | 0.9 | 250º | -1.7 |
| 200207262107 | 3.0 | 2.1 | 110º | 4.3 |
| 200212160532 | 2.8 | 3.0 | 120º | 0.3 |
| 200302280702 | 2.6 | 1.0 | 160º | 0.0 |
| 200303021718 | 2.9 | 1.8 | 150º | 0.0 |
| 200305051053 | 3.1 | 2.4 | 130º | -1.6 |
| 200306122333 | 2.6 | 0.8 | 130º | 2.1 |
| 200307191422 | 2.5 | 0.2 | 350º | -0.5 |
| 200310141045 | 2.5 | 0.8 | 140º | -1.1 |
| 200312222350 | 3.0 | 0.1 | 130º | -0.5 |
| 200407200913 | 3.1 | 1.5 | 120º | 0.6 |
| **Average** | | **1.4 km** | **156º** | **0.2 km** |

**Table 3.a.: Data pertaining to Fault Plane Solutions of Group I (no data available for the shaded spaces)**

| | | | | | | UP(1) / DOWN(2) | | | | | | | |
|---|---|---|---|---|---|---|---|---|---|---|---|---|---|
| **Event #** | **Date** | **M** | **Plane[(1)]** | **Strike** | **Dip** | **RGR** | **MGS** | **SVS** | **ΣCSU** | **HBF** | **TWB** | **WAS** | **DRC** |
| 1 | 19910424 | 1.6 | FP | N45°W ± 15° | 50° ± 23° (SW) | **1** | **1** | **2** | **2** | **2** | **1** | | |
| | | | AP | N39°E ± 15° | 82° ± 23° (SE) | | | | | | | | |
| 2 | 19831106 | 3.3 | FP | N40°W ± 10°[(2)] | 70° ± 10°[(2)](NE) | | **2** | | **1** | | | **1** | **1** |
| | | | AP | N35°E ± 10°[(2)] | 40° ± 10°[(2)] (NW) | | | | | | | | |
| 3 | 19890602 | 2.3 | FP | N27°W ± 10° | 56° ± 5° (SW) | **1** | **1** | **1** | **2** | **2** | **2** | **2** | |
| | | | AP | N15°W ± 10° | 35° ± 5° (NE) | | | | | | | | |
| 4 | 19900207 | 2.2 | FP | N30°W ± 10° | 60° ± 10° (SW) | **1** | | **2** | **2** | **2** | **1** | **2** | |
| | | | AP | N37°E ± 10° | 56° ± 10° (SE) | | | | | | | | |
| 5 | 20011223 | 2.8 | FP | N30°W ± 13° | 46° ± 23° (SW) | **2** | **1** | **2** | **2** | **2** | | **2** | **2** |
| | | | AP | N15°W ± 13° | 45° ± 23° (NE) | | | | | | | | |
| 6 | 19901113 | 2.9 | FP | N42°W ± 20° | 56° ± 13° (NE) | **2** | **2** | **2** | **2** | | **2** | **2** | |
| | | | AP | N5°W ± 20° | 40° ± 13° (SW) | | | | | | | | |
| 7 | 19910115 | 2 | FP | N45°W ± 15° | 60° ± 35° (SW) | **2** | **1** | **2** | **2** | **2** | **1** | **2** | |
| | | | AP | N29°E ± 15° | 64° ± 35° (SE) | | | | | | | | |
| 8 | 19881213 | 2.3 | FP | N20°W ± 15° | 75° ± 8° (SW) | **1** | | **1** | **2** | **1** | | | **1** |
| | | | AP | N75°W ± 15° | 25° ± 8° (NE) | | | | | | | | |
| 9 | 19971126 | 2.5 | FP | N30°W ± 10° | 30° ± 3° (SW) | **2** | **2** | **2** | **2** | **2** | | **2** | **1** |
| | | | AP | N74°W ± 10° | 67° ± 3° (NE) | | | | | | | | |
| 10 | 19920821 | 4.1 | FP | N22°W ± 5° | 59° ± 5° (SW) | **1** | **1** | **1** | **2** | **1** | **2** | **2** | **2** |
| | | | AP | N10°W ± 5° | 26° ± 5° (NE) | | | | | | | | |
| | | | | | **Average:** | **1.4** | **1.4** | **1.7** | **1.9** | **1.7** | **1.5** | **1.9** | **1.4** |

**Table 3.b.: Data pertaining to Fault Plane Solutions of Group II (no data available for the shaded spaces)**

| | | | | | | UP(1) / DOWN(2) | | | | | | | |
|---|---|---|---|---|---|---|---|---|---|---|---|---|---|
| **Event #** | **Date** | **M** | **Plane** | **Strike** | **Dip** | **RGR** | **MGS** | **SVS** | **ΣCSU** | **HBF** | **TWB** | **WAS** | **DRC** |
| 11 | 20010722 | 2.3 | FP | N17°E ± 8° | 80° ± 13° (NW) | **2** | **1** | **2** | **2** | **2** | **2** | | |
| | | | AP | N75°W ± 8° | 80° ± 13° (SW) | | | | | | | | |
| 12 | 20000507 | 1.3 | FP | N16°E ± 5° | 72° ± 20° (SE) | | **1** | **2** | **1** | **2** | **2** | | **2** |
| | | | AP | N65°W ± 5° | 65° ± 20° (SW) | | | | | | | | |
| 13 | 19980911 | 2.1 | FP | N10°W ± 3° | 54° ± 10° (SW) | **1** | **2** | **1** | | **1** | **2** | **1** | **2** |
| | | | AP | N60°E ± 3° | 65° ± 10° (SE) | | | | | | | | |
| 14 | 20020726 | 3 | FP | N5°W ± 3° | 60° ± 10° (W) | **2** | **1** | **2** | **1** | **2** | **2** | **2** | **1** |
| | | | AP | N85°W ± 3° | 90° ± 10° (S) | | | | | | | | |
| 15 | 20001019 | 2 | FP | N20°E ± 10° | 40° ± 5° (SE) | **1** | **2** | **1** | **1** | **2** | **2** | **1** | **2** |
| | | | AP | N5°W ± 10° | 53° ± 5° (W) | | | | | | | | |
| 16 | 20040720 | 3.1 | FP | N20°E ± 5° | 70° ± 5° (SE) | **1** | | **1** | **1** | **2** | | **1** | **2** |
| | | | AP | N48°E ± 5° | 22° ± 5° (NW) | | | | | | | | |
| 17 | 19991101 | 2.4 | FP | N10°E ± 8° | 30° ± 0° (SE) | **1** | **2** | **1** | **2** | **2** | **2** | | **2** |
| | | | AP | N2°W ± 8° | 61° ± 0° (W) | | | | | | | | |
| | | | | | **Average:** | **1.3** | **1.5** | **1.4** | **1.3** | **1.9** | **2.0** | **1.3** | **1.8** |

(1) FP: Fault Plane; AP: Auxiliary Plane

(2) Estimated

**Table 3.c.: Comparison of results for Group I and Group II**

| | **Average Designated value*** | | | |
|---|---|---|---|---|
| | Group I | Group II | Difference | # of earthquakes considered |
| RGR | 1.4 | 1.3 | 0.1 | 15 |
| MGS | 1.4 | 1.5 | 0.1 | 14 |
| SVS | 1.7 | 1.4 | 0.3 | 16 |
| ΣCSU | 1.9 | 1.3 | 0.6 | 16 |
| HBF | 1.7 | 1.9 | 0.2 | 16 |
| TWB | 1.5 | 2.0 | 0.5 | 12 |
| WAS | 1.9 | 1.3 | 0.6 | 12 |
| DRC | 1.4 | 1.8 | 0.4 | 11 |

* 1 if first arrival is compressional; 2 if first arrival is dilatational

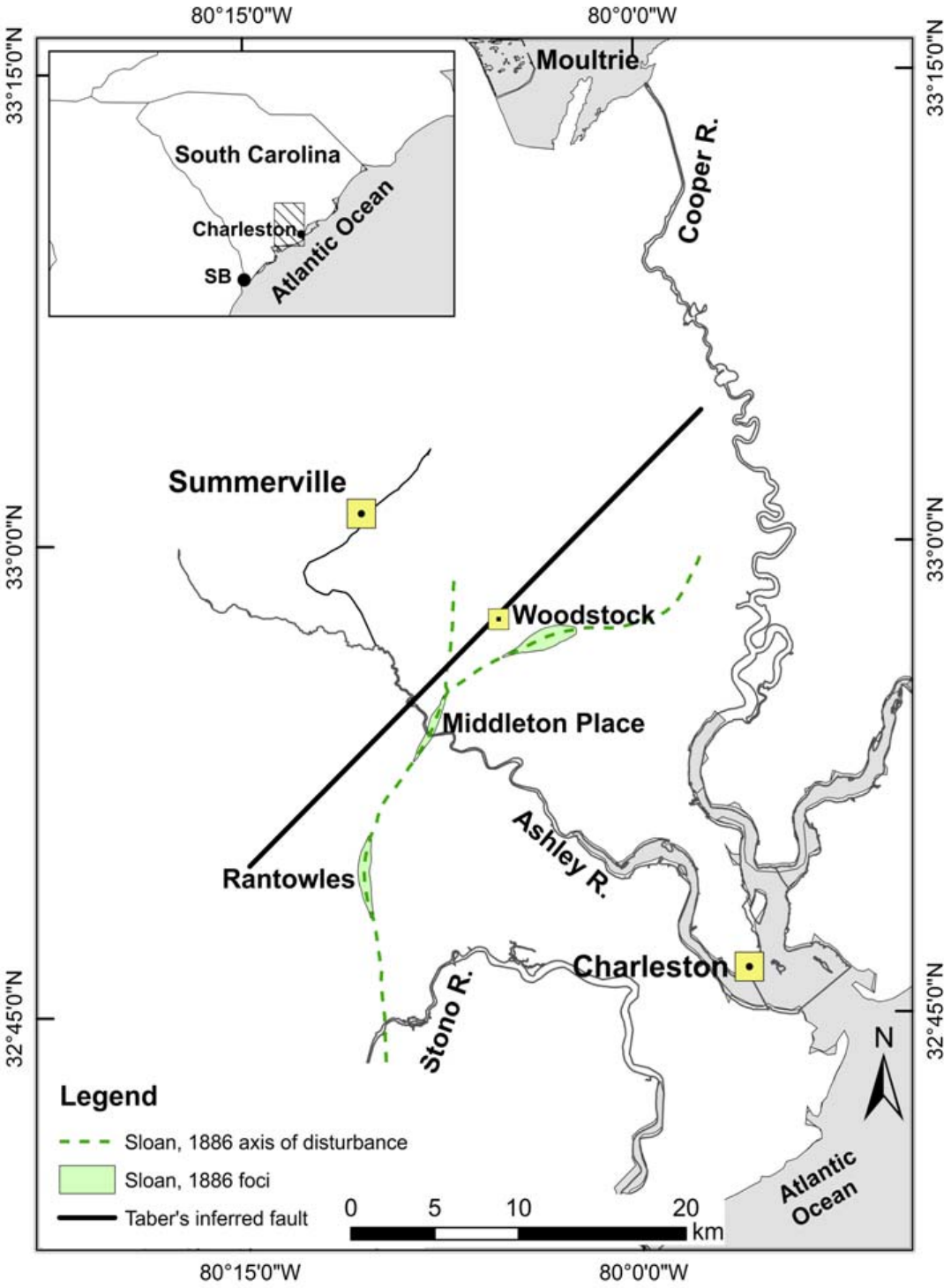


Figure 1: The three foci of the 1886 Charleston earthquake (Woodstock, Middleton Place and Rantowles) according to Sloan (in McKinley, 1887). Taber's inferred fault (Taber, 1914) for that earthquake is shown with a bold line.

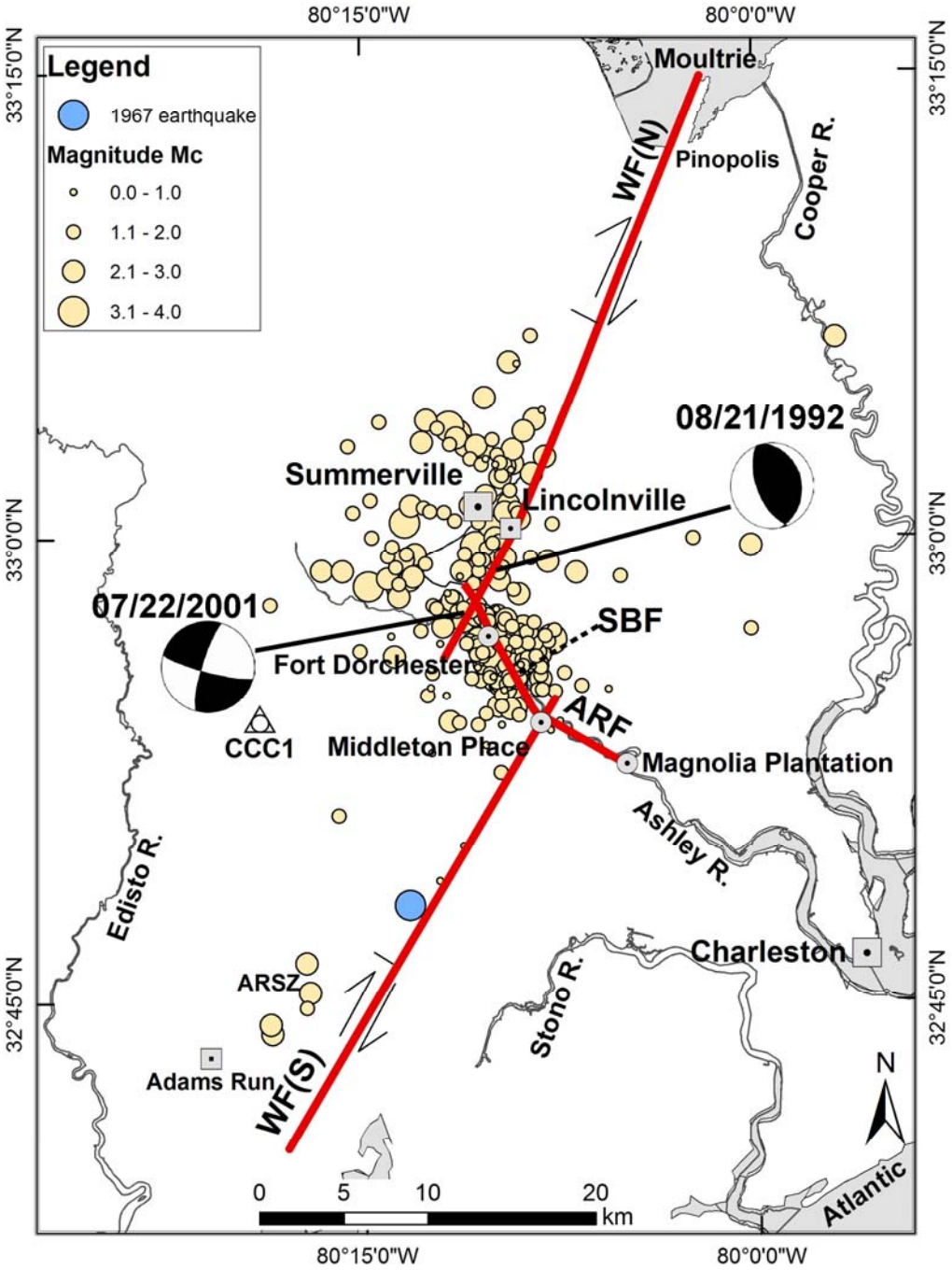


Figure 2: Epicentral locations (cream color circles) showing A and B quality microearthquakes between 1974 and 2004 and fault plane solutions of the 08/21/1992 M 4.1 and the 07/22/2001 M 2.3 earthquakes. The dense cluster of seismicity surrounding Fort Dorchester has been named the Middleton Place Summerville Seismic Zone (Tarr et al., 1981). The blue dot shows the location of the October 23, 1967, M3.4 earthquake (Dewey, 1983). The red bold lines show the seismotectonic framework according to Durá-Gómez (2004). The framework consists of the NE trending Woodstock fault (WF) which is cut and offset to the NW along the Sawmill Branch fault (SBF).

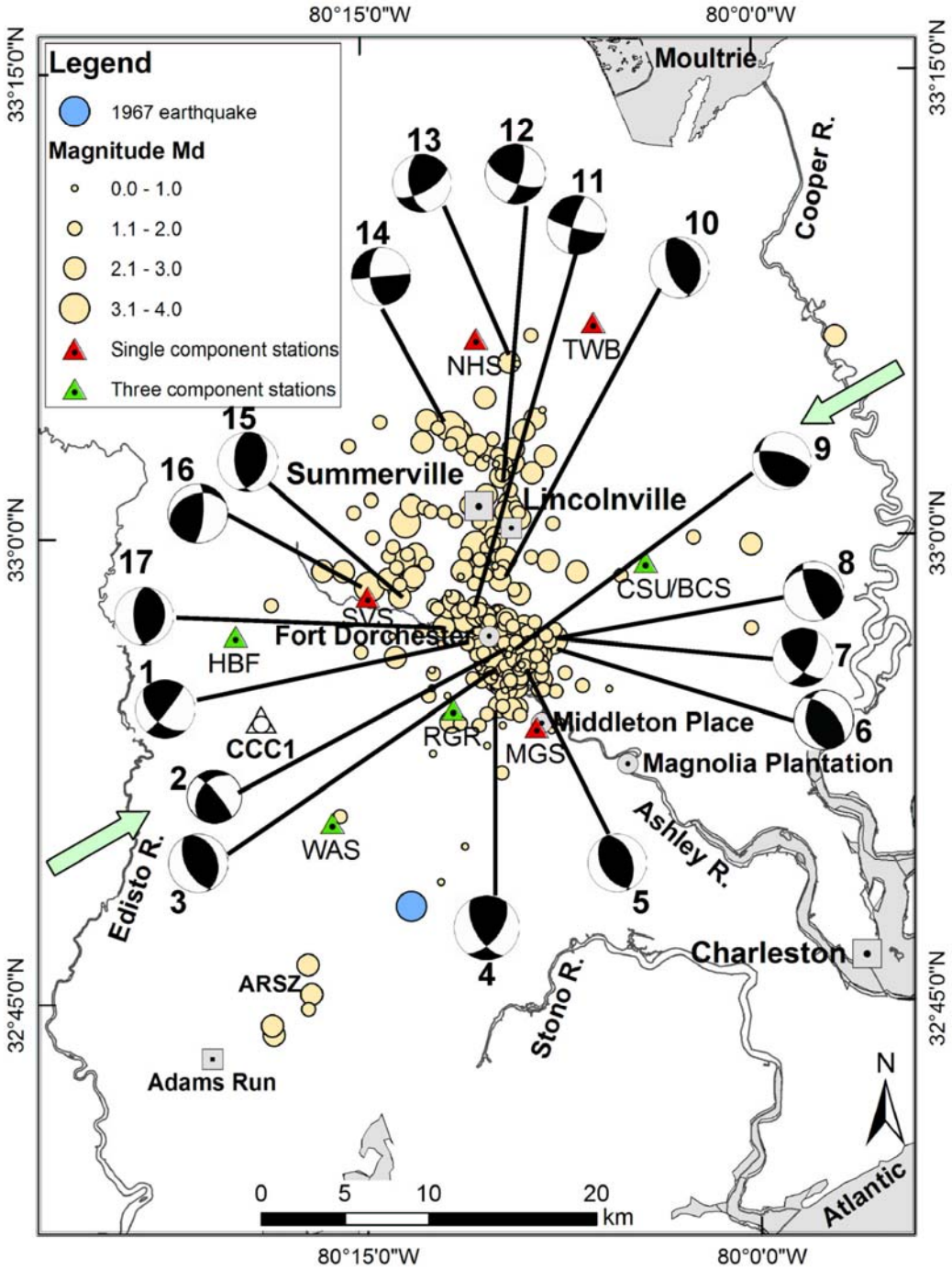


Figure 3: Seismicity for the period 1974 to 2004 (quality A and B solutions using HYPOELLISE) and 17 well-constrained fault plane solutions (the strike directions are good to ≤ 15º). All solutions suggest compressional deformation with $S_{Hmax}$ oriented N60ºE (open arrows). Solutions 1-10 are predominantly associated with NW-SE trending reverse faults; and 11-17 with N-S trending strike-slip and reverse faults. Squares and circles with a dot show locations of towns and important landmarks. The epicenters located in the southwest corner define the Adams Run Seismic Zone of Tarr et al. (1981). The location of the 1967 earthquake was obtained from Dewey (1983).

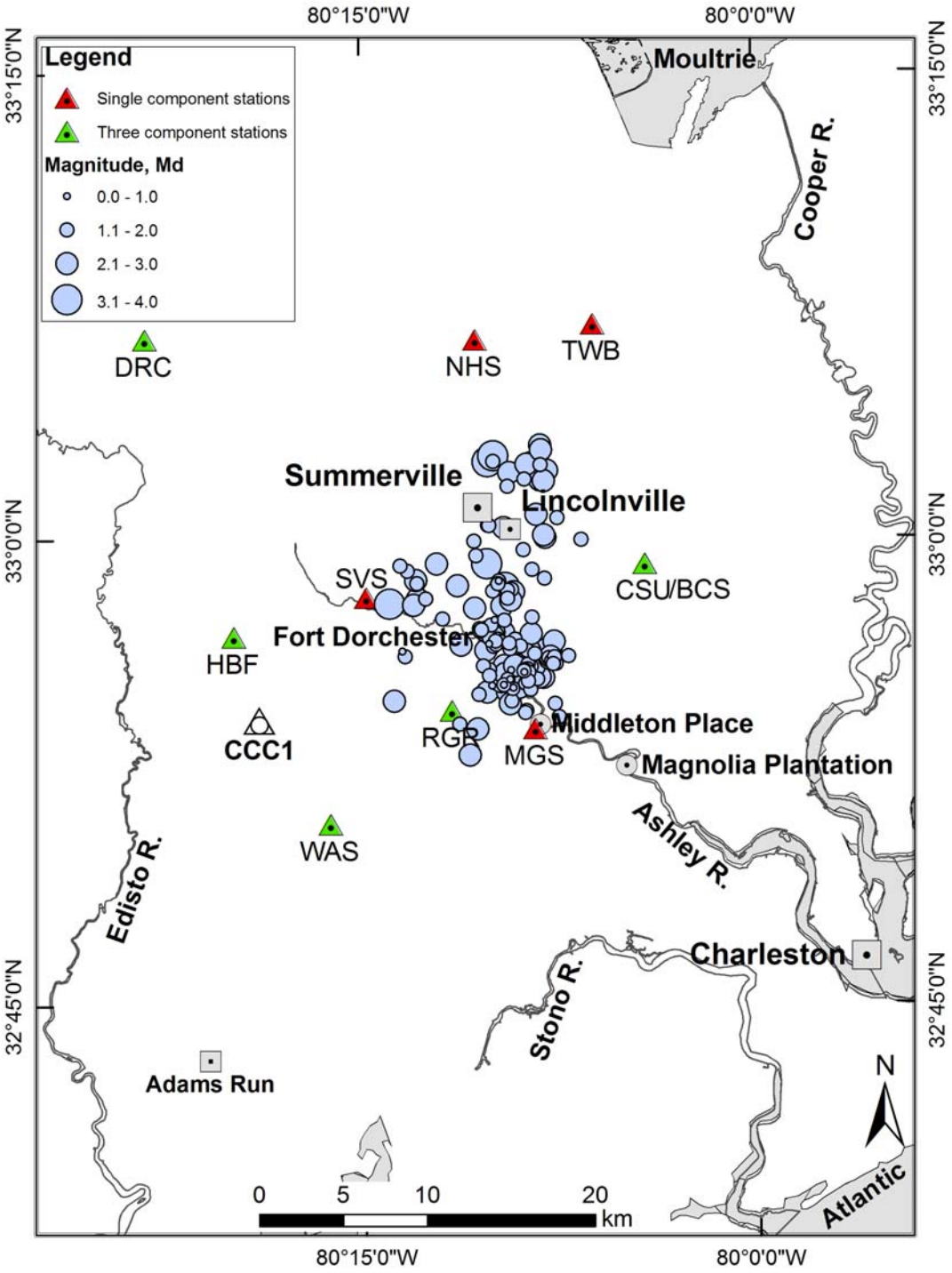


Figure 4: Relocated epicentral locations using HypoDD. Note that only about two thirds of the epicenters shown in Figure 3 could be relocated using this method.

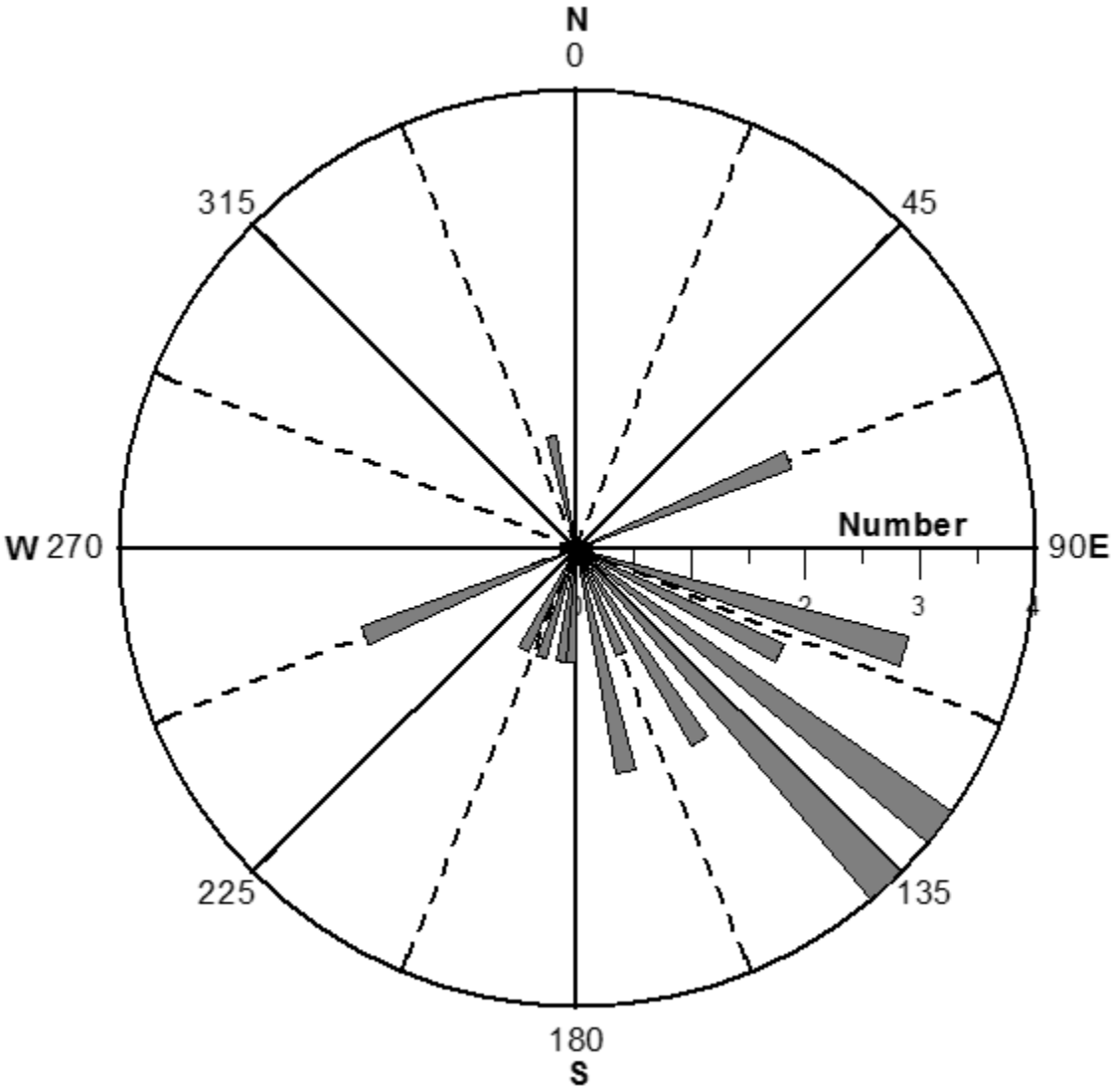


Figure 5: Rose diagram showing the angle of displacement from HYPOELLIPSE to HypoDD epicentral locations (measured from the north). The radii give the number of events.

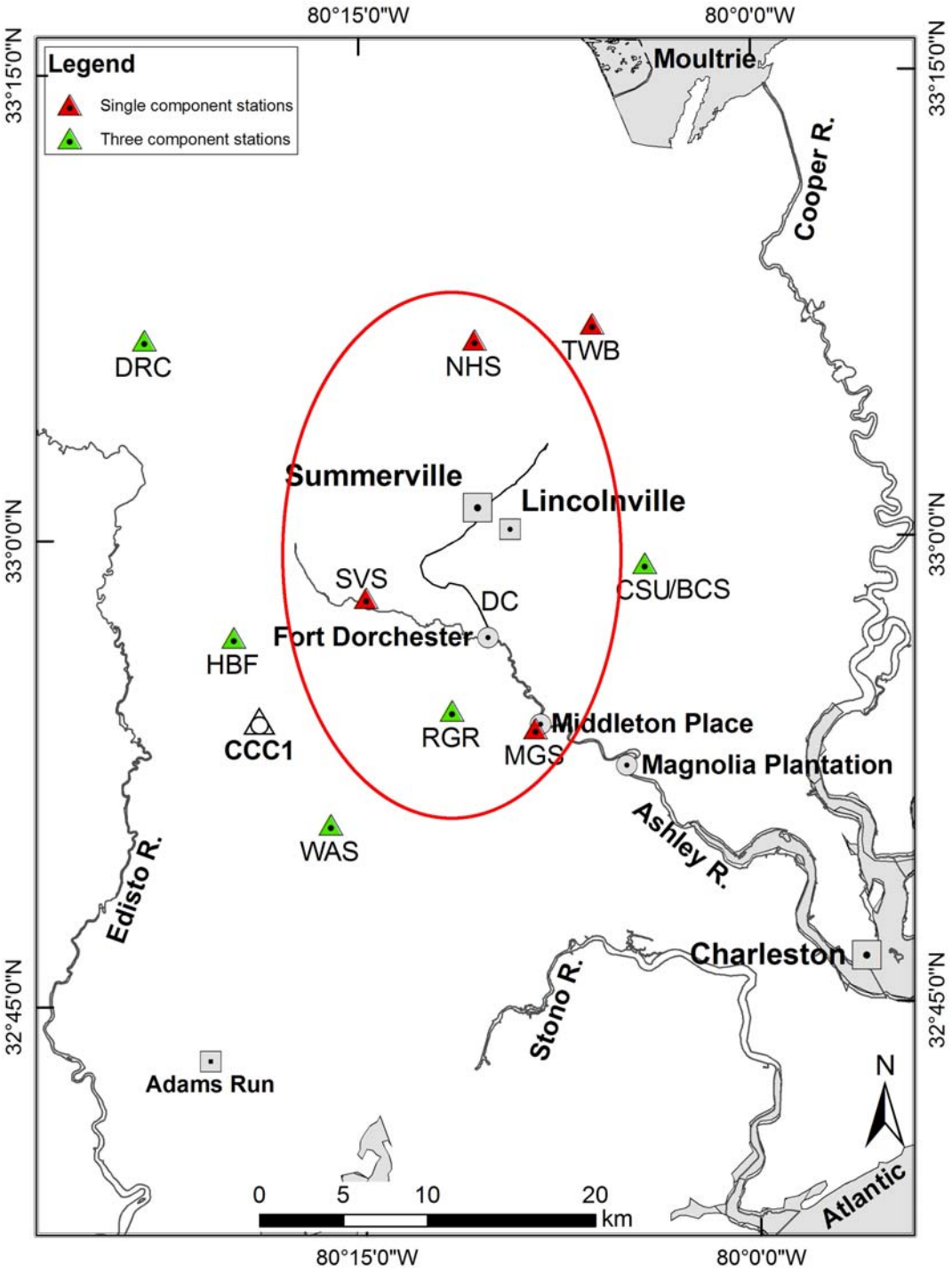


Figure 6a: Location of seismic stations and boundary of main seismicity area. SGS is located (33.1925ºN, 80.5095ºW) outside the figure. NHS, TWB and HWD were deactivated in 1980, 2006 and 1995 respectively. CCC1 shows the location of Clubhouse Crossroads well # 1. DC shows the location of Dorchester Creek, its NE continuation is called Sawmill Branch.

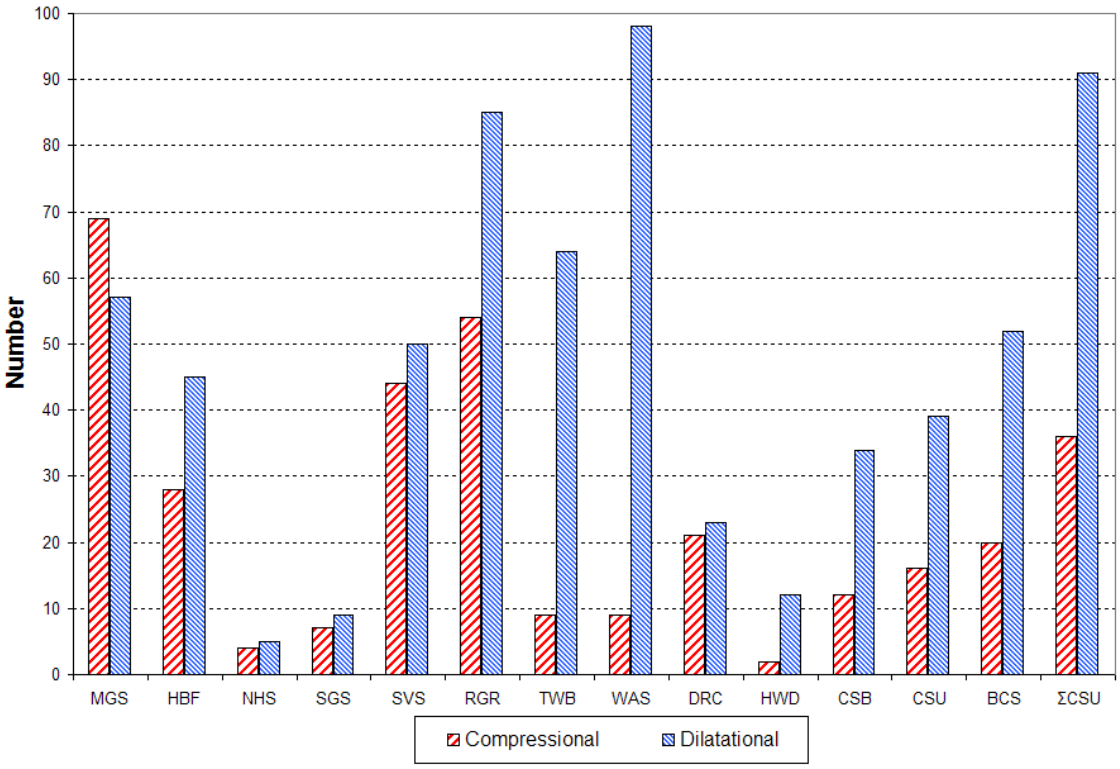


Figure 6b: Numbers of compressional and dilatational first arrivals by station for all earthquakes located by HypoDD. ΣCSU is the sum of CSU and BCS.

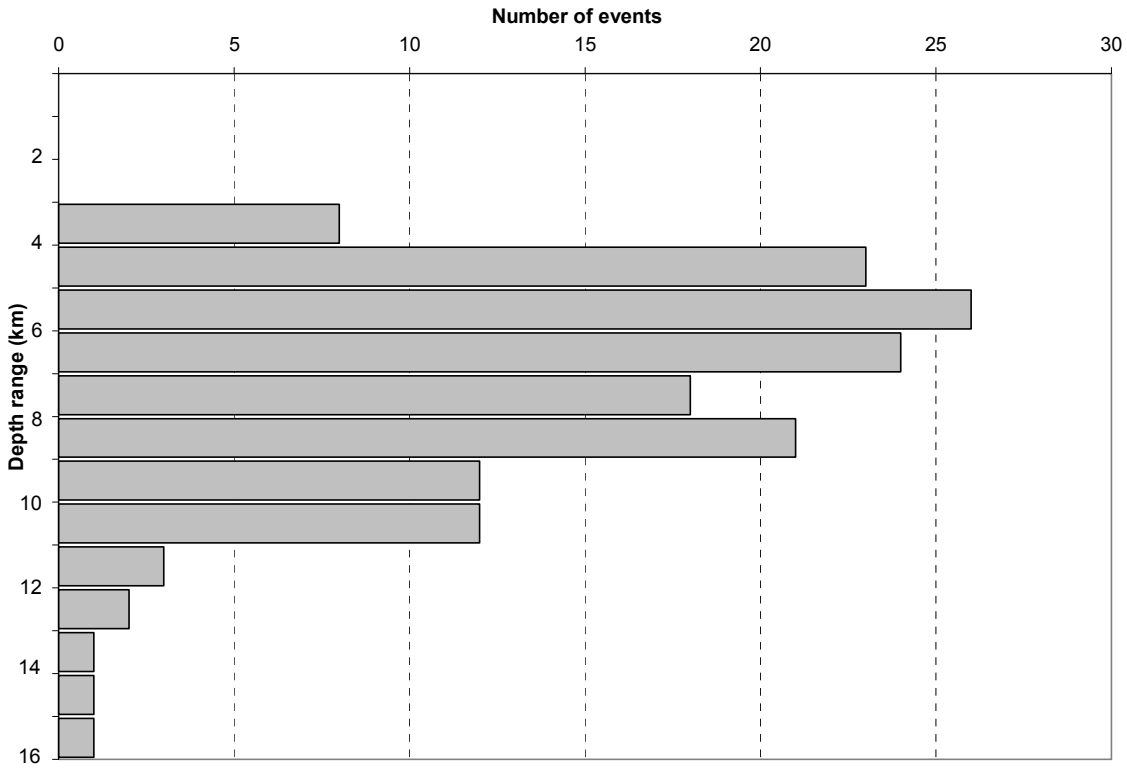


Figure 7: Depth distribution of earthquakes (using HypoDD). Most of the hypocenters lie between 3 and 13 km depth.

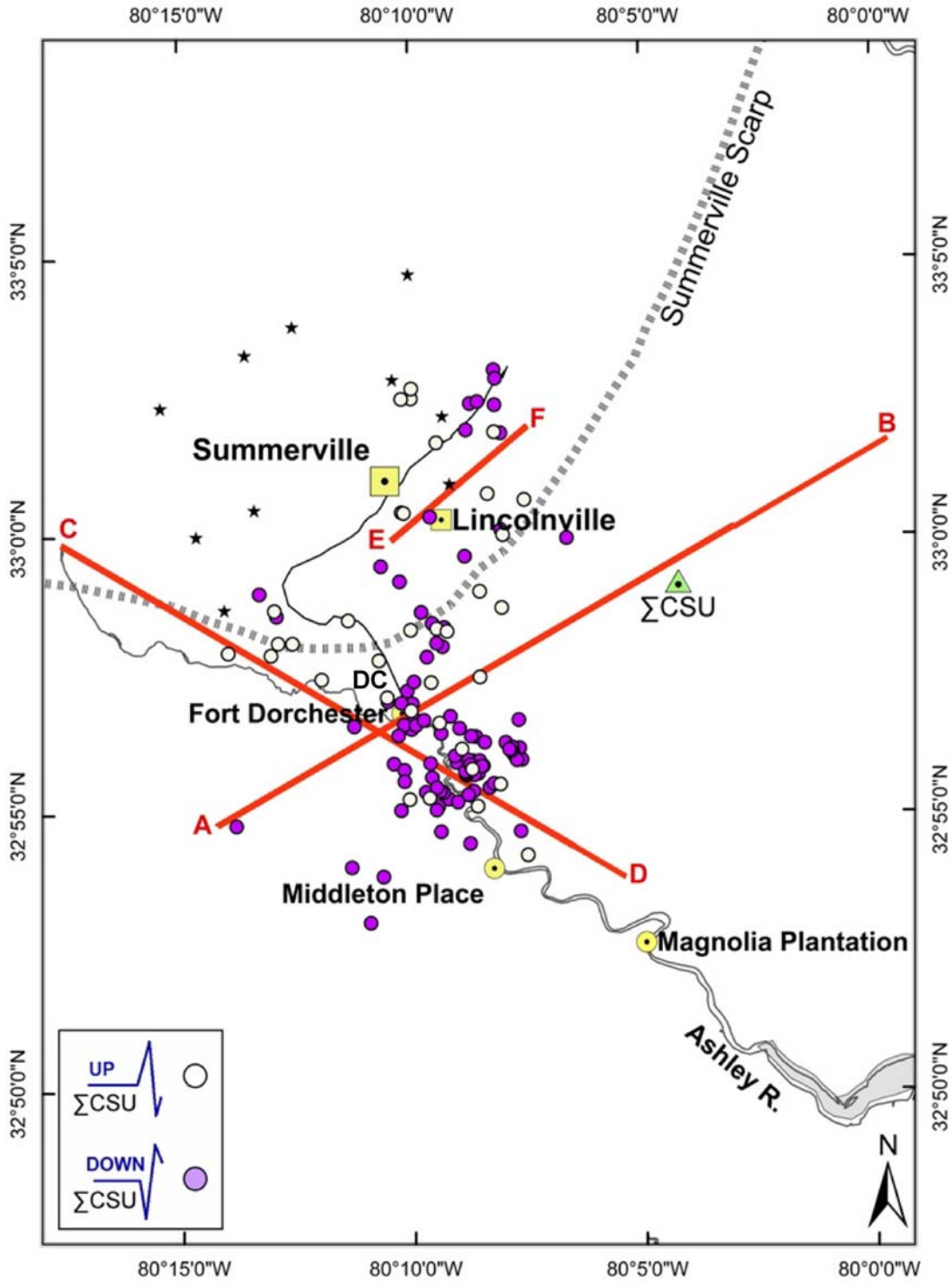


Figure 8: Epicentral locations obtained from HypoDD. Earthquakes with compressional and dilatational first arrivals at ΣCSU are shown by open and solid circles, respectively. A and B quality locations of events obtained by HYPOELLIPSE north of the Summerville scarp are shown by stars. DC shows the location of Dorchester Creek. Cross-sections were obtained along AB, CD and EF (see text for details).

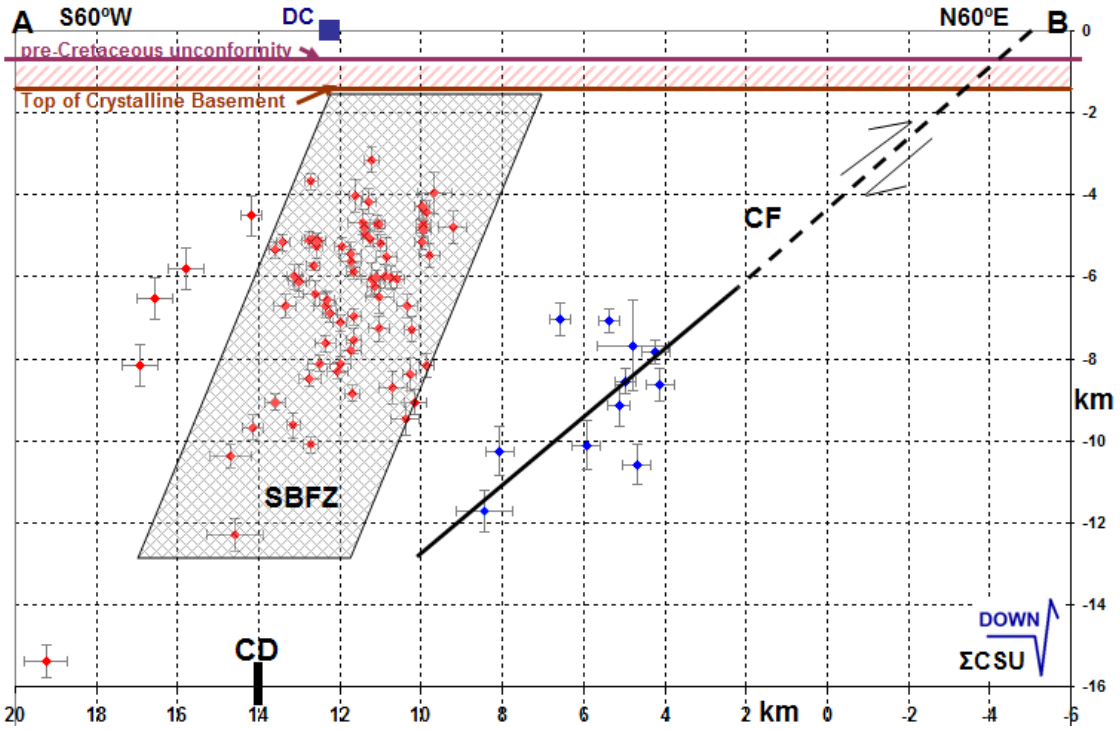


Figure 9a: Cross-section along AB (Figure 8) oriented S60°W–N60°E showing earthquakes with dilatational first arrivals at ΣCSU (solid circles in Figure 8), that define the Sawmill Branch fault zone (SBFZ) and the Charleston fault (CF). The shaded area in red shows the interpreted location of basalt flows and intercalated sediments. A preliminary interpretation suggests a ~70° SW dip for SBFZ and a ~40° SW dip for CF. DC (blue square) on the surface shows the location of Dorchester Creek. CD shows where the cross-section along CD intersects the present cross-section.

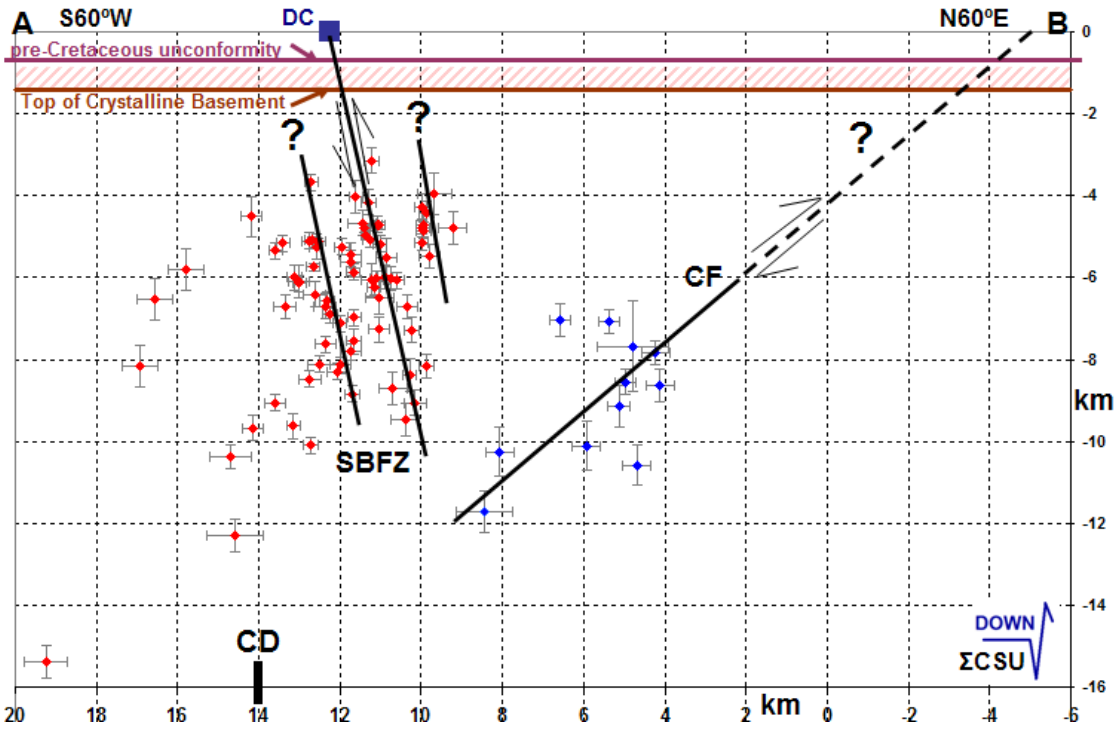


Figure 9b: An alternate interpretation of the cross-section along AB suggests the presence of a series of parallel faults in the SBFZ dipping steeply to the NE, while the CF dips about 40° to the SW. The shaded area in red shows the interpreted location of basalt flows and intercalated sediments. DC (blue square) on the surface shows the location of the Dorchester Creek. CD shows where the cross-section along CD intersects the present cross-section.

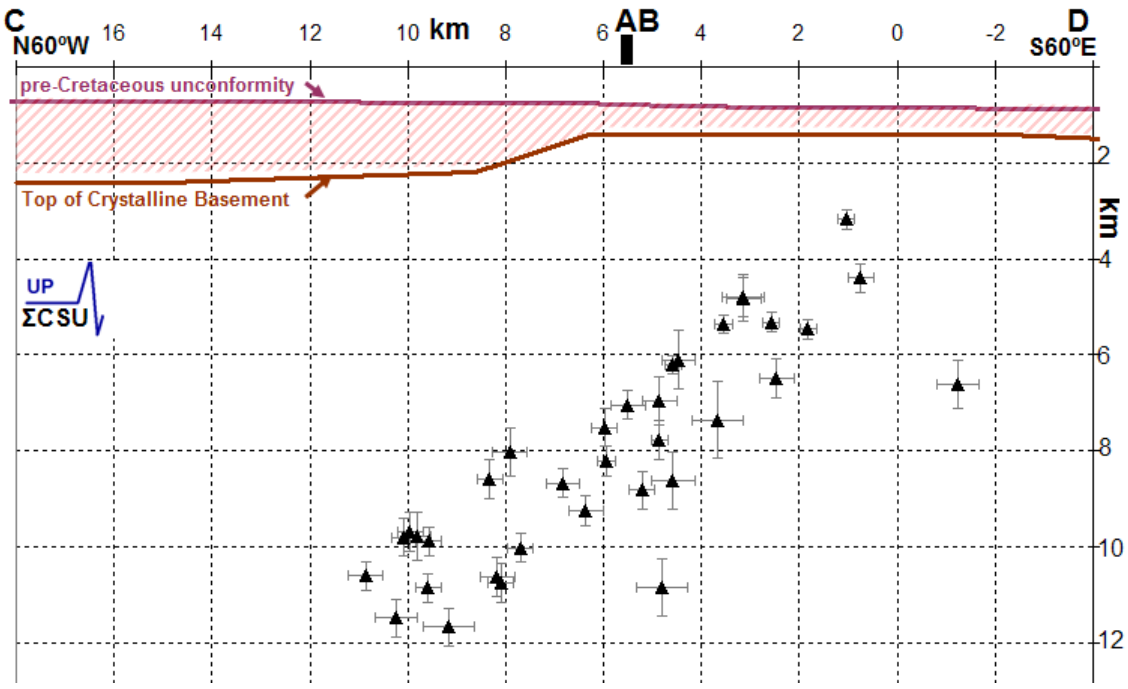


Figure 10: Cross-section along CD (Figure 8) oriented N60°W-S60°E, showing only compressional arrivals at ΣCSU (open circles in Figure 8). The shaded area is the inferred location of basalt flows and intercalated sediments. AB shows where the cross-section along AB intersects the present cross-section.

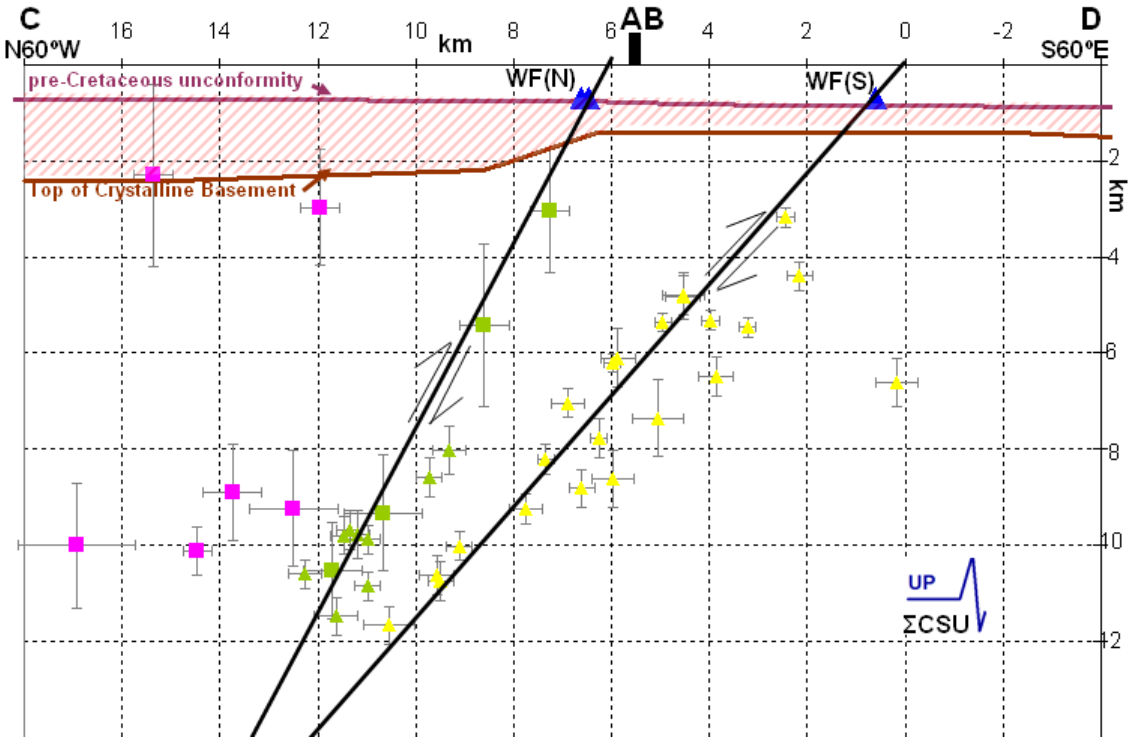


Figure 11a: Cross-section along CD (Figure 8) showing earthquakes with compressional first arrival at ΣCSU. Earthquakes located by using HypoDD, and A and B quality hypocentral locations obtained with HYPOELLIPSE are shown by triangles and squares respectively. The colors are coordinated with their epicentral locations shown in Figure 13. Earthquakes associated with WF(N), green, lie to the N and W of the Ashley River, whereas those with WF(S), yellow, lie along the Ashley River and to its south. Earthquakes located using HypoDD have been translated 1.4 km to the NW to compare with the absolute locations given by HYPOELLIPSE and supplementary data. The shaded area shows the interpreted location of basalt flows and intercalated sediments. The faults mapped in the basalt are shown as blue triangles. This and other complementary data suggest that the surface expression of the WF(S) is located at ~ (0, 0) km while the surface expression of WF(N) is located at ~ (6.3, 0) km. WF(S) dips about 50° to the NW. The inferred location of both WF(S) and WF(N) at the surface is in agreement with corroborative data on the basalt flows (700 m depth) and surface geology (see companion paper). The dip of WF(N) is not well constrained. AB shows where the cross-section along AB intersects the present cross-section.

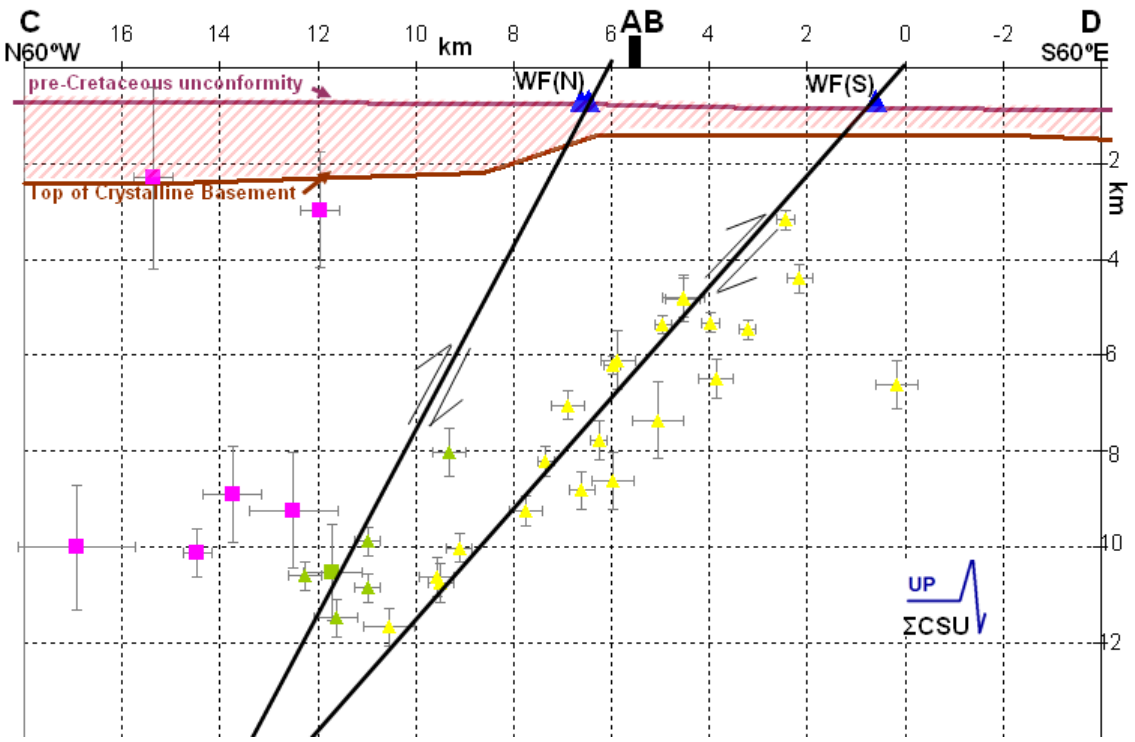


Figure 11b: Resulting cross-section along EF after the removal of the seven earthquakes in Figure 11a which are included Figure 12a (in green) to define the LF.

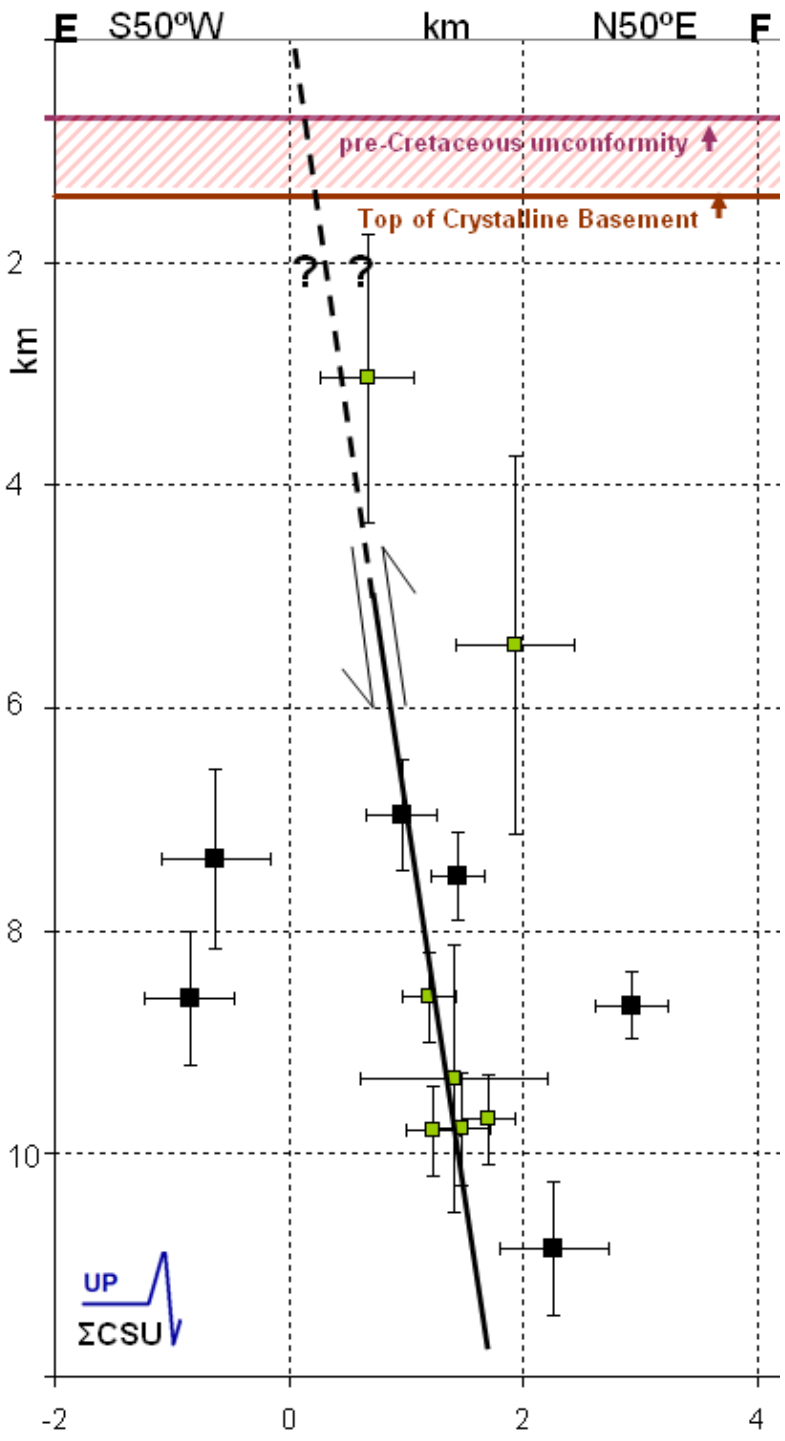


Figure 12a: Cross-section along EF (map view in Figure 8 and shown in gray and green in Figure 13). Earthquakes that were used to interpret the WF(N) (Figure 11a) are shown in green. Hypocentral locations suggest a steep (~80º) NE dipping fault, which we have named the Lincolnville fault (LF). The shaded area shows the interpreted location of basalt flows and intercalated sediments.

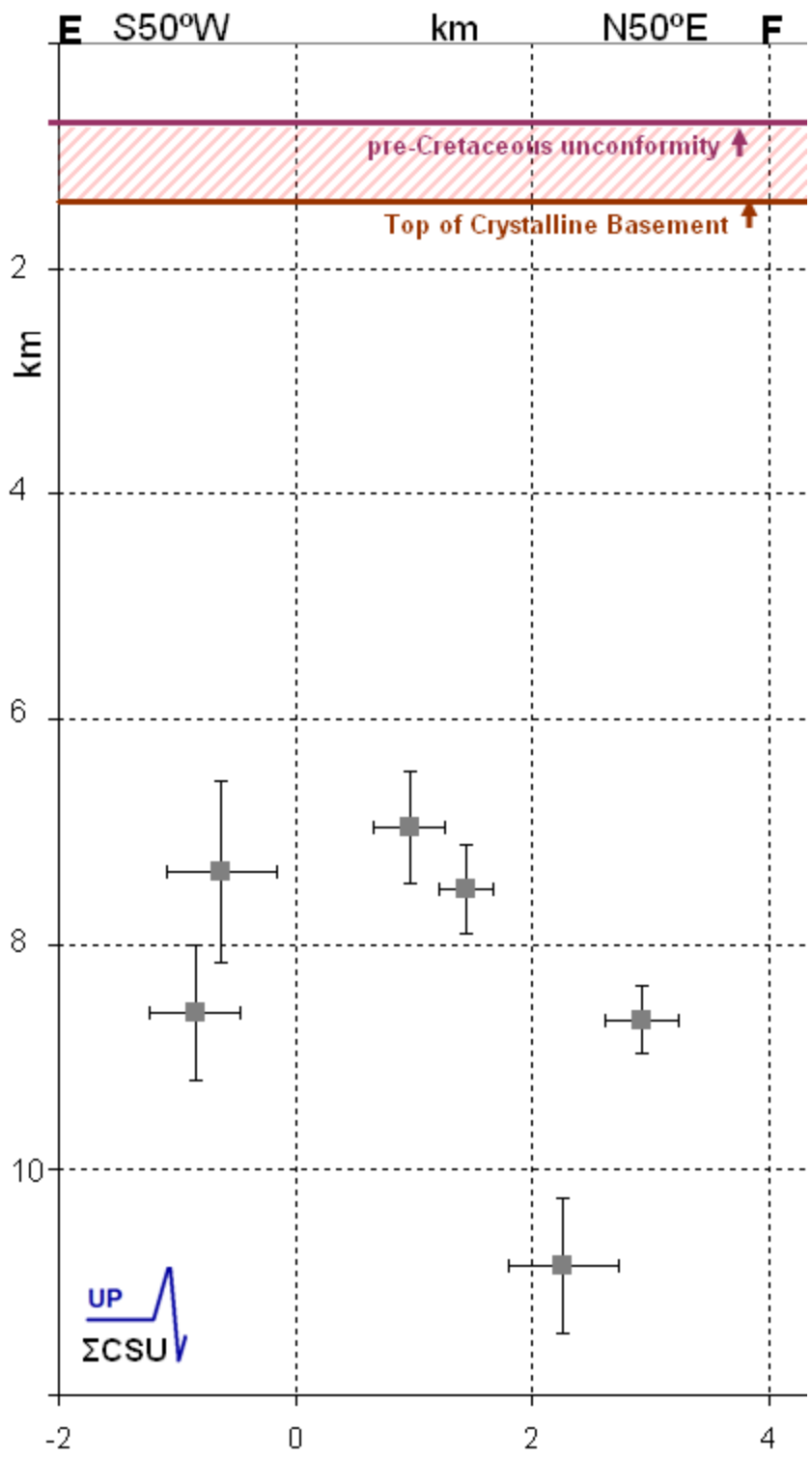


Figure 12b: Cross-section along EF (map view in Figure 8 and shown in green in Figure 13). The earthquakes that were used to describe the WF(N) in Figure 11a have been removed. The remaining hypocentral locations are too few do define a fault plane(s). The shaded area shows the interpreted location of basalt flows and intercalated sediments.

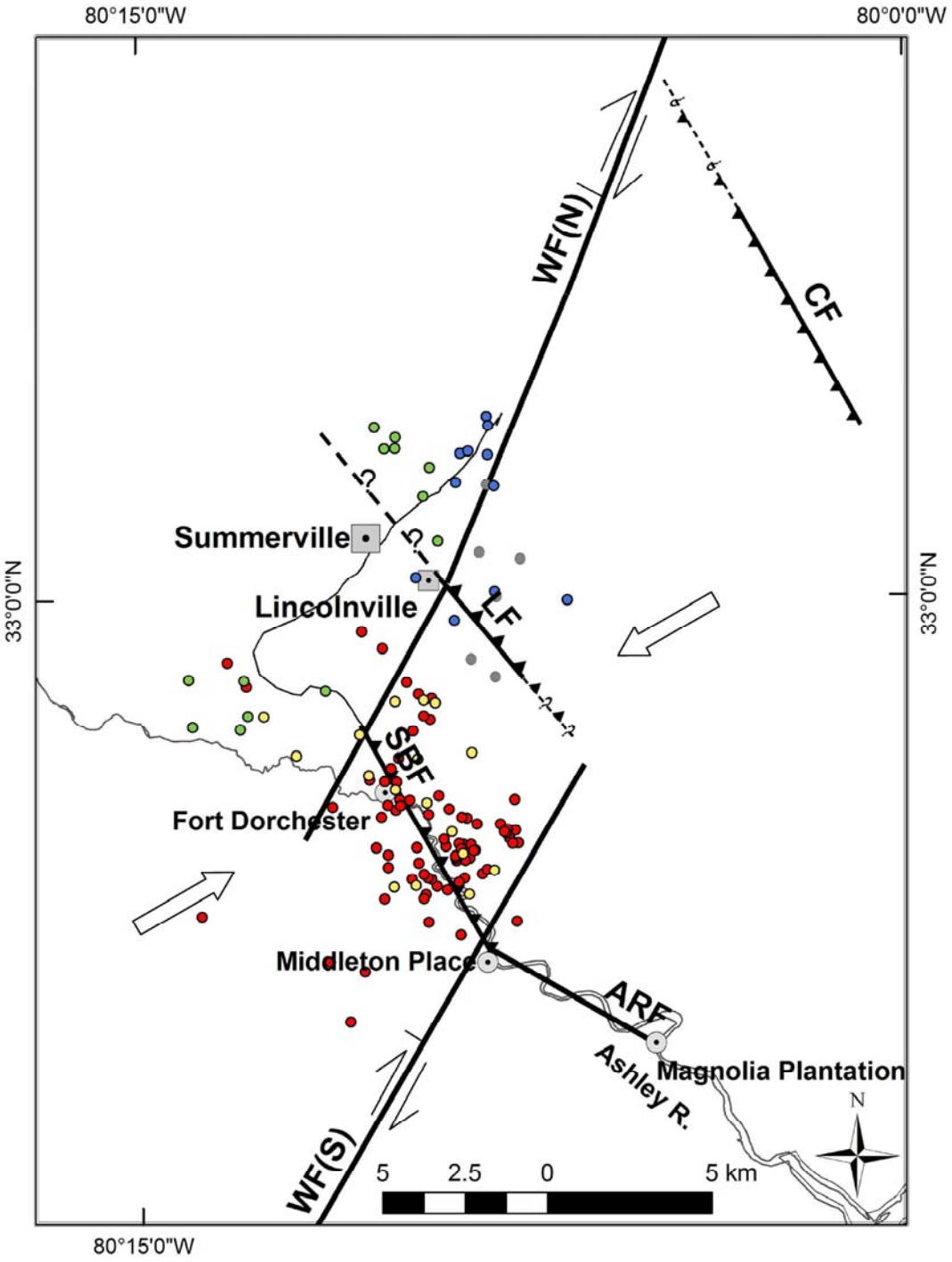


Figure 13: Close up view of the revised seismotectonic framework based on the analysis of seismological data showing the inferred faults and the earthquakes used to define them. The epicentral locations of the earthquakes are color-coordinated with the different faults interpreted here, and in the cross sections (Figures 9-12). They are WF(S) (yellow), WF(N) (green), SBF (red), CF (blue), and LF fault (gray). For the epicenters shown in red and blue the first arrival at CSU was down and for those shown in gray, green and yellow, it was up. Open arrows show the $S_{Hmax}$ direction, N60°E. We prefer the NE dip for the SBFZ as discussed in the text. The figure shows the most prominent styles of faulting.

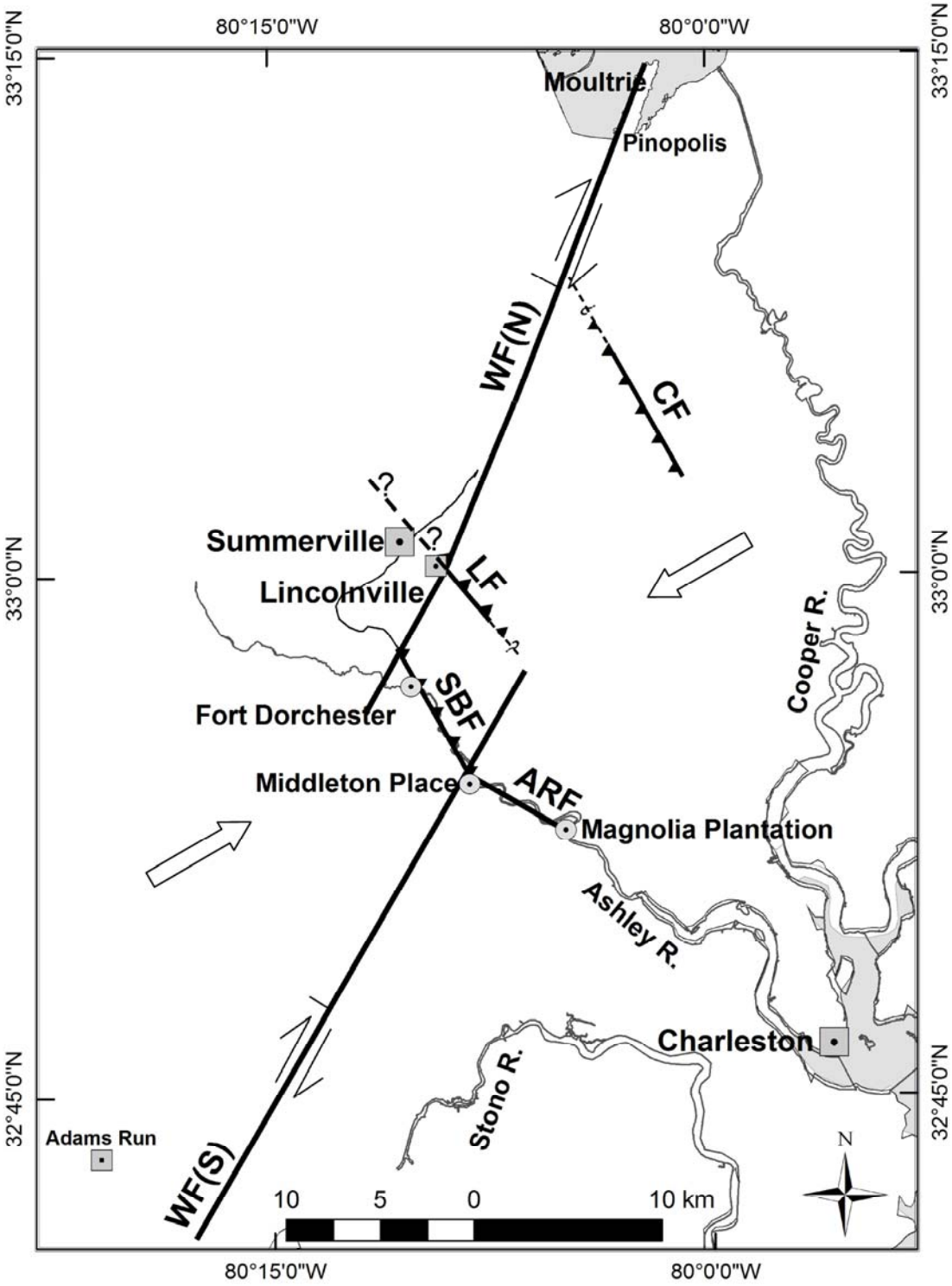


Figure 14: The revised seismotectonic framework. WF(N) continues NE to Pinopolis, and WF(S) continues SW to the Adams Run Seismic Zone near a town by that name.

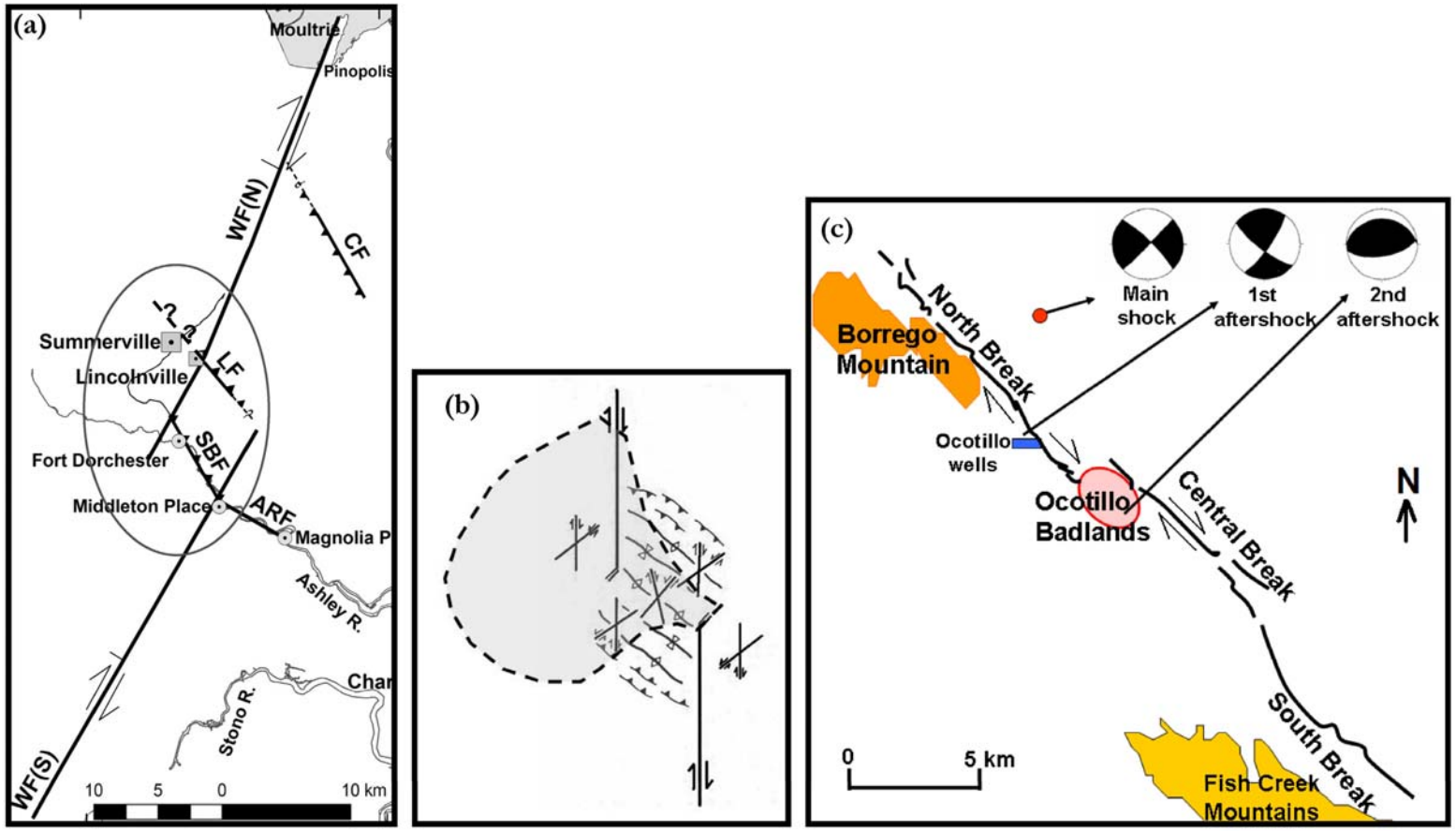


Figure 15: Comparison of the (a) seismotectonic framework of the MPSSZ with (b) the analysis of Sibson (1986) for antidilational jogs and (c) the style of faulting of the 1968 Borrego mountain earthquake and its aftershocks, modified from Burford (1968) and Burdick and Mellman (1976). The ellipse in (a) shows the boundary of the MPSSZ seismogenic area. In antidilational jogs Sibson reports compression associated with folds and thrusts, as well as large aftershock distributions (shaded area). Our interpretation of the seismotectonic framework for MPSSZ, a right-lateral strike-slip fault with a left-step associated with a series of steeply dipping reverse faults with opposing dips, agrees with the analysis of Sibson (1986) for the style of faults with an antidilational left-stepping jog. The style of faulting at Charleston, right-lateral on WF and (primarily) reverse on SBF, is similar to that observed from the Borrego Mountain earthquake.